HYDROGEOPHYSICAL EVIDENCE OF GROUNDWATER CONVECTION IN THE NACIMIENTO FAULT

By

ROBERT REYNOLDS

Bachelor of Arts in Psychology, Fine Arts

University of Colorado, Colorado Springs

Colorado Springs, Colorado

2001

Submitted to the Faculty of the
Graduate College of the
Oklahoma State University
in partial fulfillment of
the requirements for
the Degree of
MASTER OF SCIENCE
July, 2013

HYDROGEOPHYSICAL EVIDENCE OF GROUNDWATER CONVECTION IN THE NACIMIENTO FAULT

Thesis Approved:

Dr. Todd Halihan

Thesis Adviser

Dr. Lowell Caneday

Committee Chair

Dr. Eliot Atekwana

Committee Member

TABLE OF CONTENTS

LIST OF FIGURES

ACKNOWLEDGMENTS

This project would not have been possible without the support of numerous individuals. I would like to thank my advisor, Todd Halihan, for providing training and insight into the equipment used in the research, and his time provided in and out of the field. I would also like to thank the other members of my committee, Dr. Caneday, who helped to provide the opportunity to continue my education, and also Dr. Atekwana for joining the committee at a later stage.

The financial support received from the Oklahoma State University Environmental Science Graduate Program in the form of a Public Service of Oklahoma Research Assistantship is greatly appreciated. The Geological Society of America research grant I received also made it possible for the research to be completed by supporting the field data collection expenses.

I would like to thank the Oklahoma State University Boone Pickens School of Geology for the use of their facilities. Thanks go to Karl Karlstrom and Laura Crossey from the University of New Mexico for their support and lodging assistance, and to the University of New Mexico students Chad Bryant, Christopher McGibbon, Pavel Vakhlamov, and New Mexico Tech student Ken Salaz for their work during the field data acquisition.

Acknowledgements reflect the views of the author and are not endorsed by committee members of Oklahoma State University.

ABSTRACT

Theory exists for unstable convective motion in porous and fractured media, and has been detected in the field as fluid fingers in porous media. Groundwater convective theory is limited though due to a lack of field evidence to understand and quantify the process of free convection in other settings such as faults. The Nacimiento Fault Zone in New Mexico was a suitable location for such a field study. This work provides quantification of haline convection in a hydraulically active fault zone. The hypothesis proposed that measured convective parameters of wavelength and timescales obtained from electrical resistivity and fluid data will correlate to convective groundwater theory in fault zones. Over a 2 year period (2011-2012), a total of 16 ERI lines provided two-dimensional and three-dimensional mapping of the convective fluid signatures in the Nacimiento Fault. Additionally, one line of transient data evaluated changes in the fault over a 6 day timescale. The results show circular conductive features which change over time as well as EC oscillations in transducer data.

CHAPTER I

INTRODUCTION

A theory of unstable convective motion in porous and fractured media has been developed (Shikaze et al., 1997; Simmons et al., 2001; Simmons et al., 2008), and the detection of free convection in porous media in the field has recently been explored (Van Dam et al., 2009). Groundwater convective theory however, is limited due to a lack of field evidence to understand and quantify the process of free convection in groundwater systems. Preliminary data from May 2011 suggested that the Nacimiento Fault Zone in New Mexico was a potential location for quantifying groundwater convection in a fault zone, where no field data exist on convective flow processes. Quantifying fluid movement and saline transport in fault zones is important for water supply and understanding geologic processes in these areas. As the site is composed of faulted shale, the understanding of these processes has additional importance as shale hydrogeology is still poorly understood. While there has been some research into the relationship between groundwater convection and geothermal anomalies along the Rio Grande rift, only circumstantial support for convection theory was found (Morgan et al., 1981). Thus, this work provides the first attempt to quantify haline convection in a hydraulically active fault zone. Based on theoretical development of Simmons et al. (2008), this study was developed to evaluate the presence of haline convection cells in a fault zone and the presence of rapidly changing salinities in a system with stable discharge. The study was conducted in two phases, a reconnaissance phase to evaluate the fault fluid structure and an evaluation phase which included a pseudo three-

dimensional geophysical investigation and a temporal geophysical investigation to determine if sufficient evidence exists to demonstrate free convection and to quantify the effect if it exists. The hypothesis proposes that measured convective parameters of wavelength and timescales obtained from electrical resistivity and fluid data will correlate to convective groundwater theory in fault zones. To develop the evidence, an understanding of free convection processes is required followed by an approach to look for this evidence in a groundwater system by choosing the correct field location and equipment. Finally, testable evidence must be generated to exclude other possible mechanisms as governing the field situation.

Free Convection

Theoretical modeling of free convection (also known as natural convection) in groundwater is limited due to a lack of field data, but is expected to affect a number of groundwater problems of interest. Numerical modeling supports speeds of free convection at decimeters to meters per day, suggesting that the timescale for the process is short and observable in the field (Simmons, 2008). Once the onset of convection occurs, density can be affected for an entire layer of groundwater in the timespan of 2-4 weeks (Simmons et al., 2001). Flow paths from landfill plumes and radioactive waste sites can be affected by differences in density, thus density-driven free convection in the field is of vital importance to contaminant transport applications (Deng et al., 2004). Field data quantifying free convective processes would significantly advance the study of groundwater convective theory, demonstrating that free convection occurs more often than previously thought (Van Dam et al., 2009). For water supply in faulted aquifers, deep faults can bring poor quality water to shallow aquifers; convective processes can further concentrate solutes impacting both surface and groundwater (Hanna and Harmon, 1989). Groundwater flow near salt domes, where the fluid is a mixture of fresh water and brine, and the evaporation of salt lakes are

examples of the need for field research in this area (Holzbecher, 1998). Quantifying these processes will allow for an increased ability to predict the impacts on current and future water supply as well as furthering the geological understanding of near surface groundwater flow. For questions of fluid flow at depth, hydrothermal fluids migrating upwards along faults could be even more unstable than other convective systems. This research may allow better insight into the hydrology of hydrocarbon reservoirs and geothermal energy systems (Rabinowicz et al., 1985; Liu et al., 1997). If convective processes are occurring in a fault zone, convection cells may occur in several modes. Based on convective theory, Mode 1 interfracture convection may occur perpendicular to the fault, Mode 2A intrafracture convection and Mode 2B intrafracture convection may occur parallel to the plane of the fault with Mode 2B being the most likely mode of convection in a low permeability layer (Simmons et al., 2008).

Field Detection of Convection

Investigating convective processes in groundwater is difficult with standard approaches using sets of wells placed into the groundwater domain. In convective systems, the patterns are spatially complex and the placement of a well may disrupt convection cells. Electrical Resistivity Imaging (ERI) is a technology which allows for the observation of subsurface fluid processes from the surface (Crook et al., 2008), thus it is well suited for this type of study. Through the use of ERI equipment and inversion processing, direct current can be injected into the subsurface, and monitored at the surface, resulting in two- or three-dimensional datasets that can be analyzed. In deep-seated fault flow systems, flow rates tend to be nearly constant; affected only by barometric effects. If convection is occurring in these systems, monitoring fluid conductivity changes may show higher rates of variability than expected from deep groundwater flowing to the surface under advective (forced convective) processes. The research hypothesis maintains that measured

convective parameters of wavelength and timescales obtained from electrical resistivity and fluid field data will correlate to convective groundwater theory in fault zones (Simmons et al., 2008).

Field Evidence of Free Convection

In porous media, Van Dam et al., (2009) used finger-shaped anomalies in resistivity data along with fluid data and theoretical estimates to indicate that convection was occurring in a sabkha near Abu Dhabi, United Arab Emirates. In a fault setting, a similar set of evidence can be developed. The best site to evaluate convection in a fault zone would have steady flow with evaporation at the surface increasing the near surface salinity gradient to increase instability and aid convection. The site should also lack alternative electrical features that could be interpreted as fingering or convection cells. At a site that meets the criteria, theoretical support can be evaluated using Simmons (2008) to evaluate the Rayleigh number criterion for the onset of convection in a faulted system. As these calculations are for homogeneous media instead of faulted media, they provide guidance on the likelihood of convection, not an absolute evaluation.

Next, two-dimensional resistivity data can be evaluated in a fault zone to look for Mode 1, Mode 2A or Mode 2B convection cells. As opposed to fingering in the data, regular circular conductors can be expected in these datasets that could be evaluated for a relationship with fluid conductivity. The wavelength of these features should be related in size to the dimensions of the fault (Simmons et al., 2001). These features may be antithetical to the fault if rotation directions are antithetical as may be the case in Mode 1 cells. Transient resistivity data should show both increases and decreases in resistivity if the fluid is rotating, and should be evident compared to a steady change in one direction or no change at all. Mode 2B cells would be the most readily evaluated as they are the most unstable and would likely have the fastest rotation to detect electrically.

Field Approach

The Nacimiento Fault Zone, and more specifically, the Tierra Amarilla mound springs site lies on Bureau of Land Management public land, thus borehole exploration would not be possible to investigate the existence of groundwater natural convection. Borehole investigation would not prove nor disprove the existence of free convection in this setting as the vertical conduits themselves would disturb the free convective processes. This site met the criteria to provide a good site for convection evaluation. The field resistivity and fluid data were evaluated to determine the structure of the convective features of the fault zone, and with the addition of data from the University of New Mexico, structural mapping was also employed in order to interpret the geologic context of the ERI data to test alternative explanations for the resulting data.

CHAPTER II

REVIEW OF LITERATURE

The literature for this investigation includes an understanding of the theoretical and field data describing free convective processes in fluids. As electrical techniques are the dominant technique thus far to quantify these processes in the field, free convective theory will be described followed by a description of ERI, followed by the approach used in the literature to use these data in order to evaluate convective processes.

Free and Forced Convection

Free convection is a transport mechanism in which a density gradient exists from a source of thermal and/or salinity differences. Forced convection, or advection, is a similar transport mechanism in which an outside source is causing the transport, as in a steep hydraulic gradient, or manmade device (Simmons, 2005). Convection in non-groundwater settings has been of interest since 1900 when Henri Bénard conducted an experiment in which a thin layer of fluid was continuously heated from below, producing thermal free convection in a regular pattern of cells later known as Bénard cells. In 1916, Rayleigh theorized that a particle hotter than its

environment encounters increasingly colder fluid as it rises, driving instability and thus convection (Lord Rayleigh, 1916). Further developments include the Rayleigh-Bénard experiment which consisted of placing a fluid between two flat horizontal conductive plates, and heating the lower plate to temperature significantly above the higher plate. Thermal expansion occurs at the lower plate resulting in a lowered density at that plate, and due to the conservation of mass, instability then occurs at a finite wavelength (Cross and Hohenberg, 1993). The Rayleigh number (Ra), describes this instability, and is a dimensionless ratio of the destabilizing buoyance force to the stabilizing dissipative force (Nield, 1994).

$$Ra = \frac{\alpha g \Delta T d^3}{k\nu}$$

where Ra = Rayleigh number (dimensionless)

α = thermal expansion coefficient (meters/^{0}C)

g = acceleration due to gravity (meters^2/second)

ΔT = change in temperature (^{0}C)

d = plate separation (meters)

k = thermal diffusivity (meters^2/second)

and ν = kinematic viscosity (meters^2/second)

When the Rayleigh number is below the critical value for a specific fluid, heat transfer occurs in the form of conduction; when it is above the critical value for that fluid, heat transfer occurs in the form of thermal convection.

Convection Experiments

In 1945, free convection theory predicted that in a steady state, square cells will form with wavelengths equal to twice the layer thickness (Horton and Rogers, 1945). This gives rise to the theory that convective circulations have width equal to twice the layer thickness.

The first significant work on transient thermal convection was done by Elder (1967), and consisted of a heat convection experiment in which a rectangular Hele-Shaw cell (two flat plates parallel to each other and separated by a small distance) was heated at its base. Six convection plumes formed, though only four cells remained towards the end of the experiment. This was an important step in convection theory, but more recently the Elder problem has been shown to be ineffective in numerical modeling due to multiple steady states stemming from a high Rayleigh number of 400 (Van Reeuwijk et al., 2009). Convection theory was furthered through the investigation of thermohaline properties in a porous medium. Nield's (1968) experiment showed that oscillatory instability is possible when a "strongly stabilizing solute gradient is opposed by a destabilizing thermal gradient, but attention is concentrated on monotonic instability".

Significant progress has also been made in the field of open-ocean convection, where recent observing technology is being used to study convection processes. Detailed observations of this process have been made in the Labrador, Greenland and Mediterranean Seas (Marshall and Friedrich, 1999). In the Southern Ocean near the Greenwich meridian, brine release during ice formation is significant enough to destabilize the water column and cause the onset of open-ocean free convection. This thermohaline convection process brings deeper, warmer water to the surface which in turn melts the ice. The surface layer increases in salinity, and a destabilizing buoyancy flux occurs that continues until the ice disappears and the cooling is no longer vigorous enough to destabilize the water column (Goosse and Fichefet, 2000).

Free convection heat transfer has also been studied in solar collectors where heat flux distributions occur in the annular space between circular receiver tubes and glass envelopes. Finite difference numerical modeling was used to obtain a Rayleigh number of $1.2 \times 10^{+04}$ (Kassem, 2007).

Spontaneously generated convection has been observed in oil drop experiments where, "monodisperse polystyrene particles with a mean diameter of 2.134 μm were added to varying concentrations of nonionic surfactant solutions" underneath a glass surface (Peña and Miller, 2006). At high surfactant concentrations, radial convection was monitored by videomicroscopy. The convection pattern in Figure 2.1 below shows circulation within the oil drop.

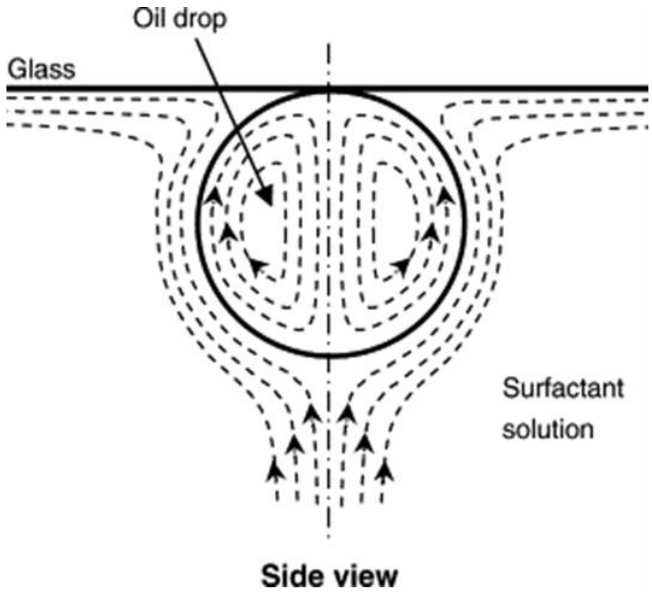

Figure 2.1: Diagram of the results of an oil drop experiment (Peña and Miller, 2006). The thermal convective cell is composed of two counter-rotating cells.

Submerged throat glass melting furnaces have also been shown to produce three-dimensional convection in the production of glassware, container glass and TV panels (Pilon et al., 2006). The glass melting furnace consists of a melting tank which is connected to the output of the melted glass by a connected channel referred to as a throat. Figure 2.2 shows the Mode 1 convective circulation pattern formed in submerged throat furnaces which have no air bubbles or electric boosting. Pilon et al., (2006) found that in an experimental glass tank 15.85 meters long, 7.32 meters wide and 1.03 meters deep, 16 Rayleigh-Bénard cells were observed in the glass batch. These convective cells extended along the entire length of the glass tank, but then dissipated as soon as the glass surface came into contact with the combustion space. A heat flux gradient in the x-direction is present, (Figure 2.3b), and is the driving force behind the two circulation loops in the longitudinal direction (Zhiqiang and Zhihao, 1997; Pilon et al., 2006). The three-dimensional convection which is produced is similar to the known Mode 1 convective cell structure, as the flow pattern is antithetical and contains fingering patterns.

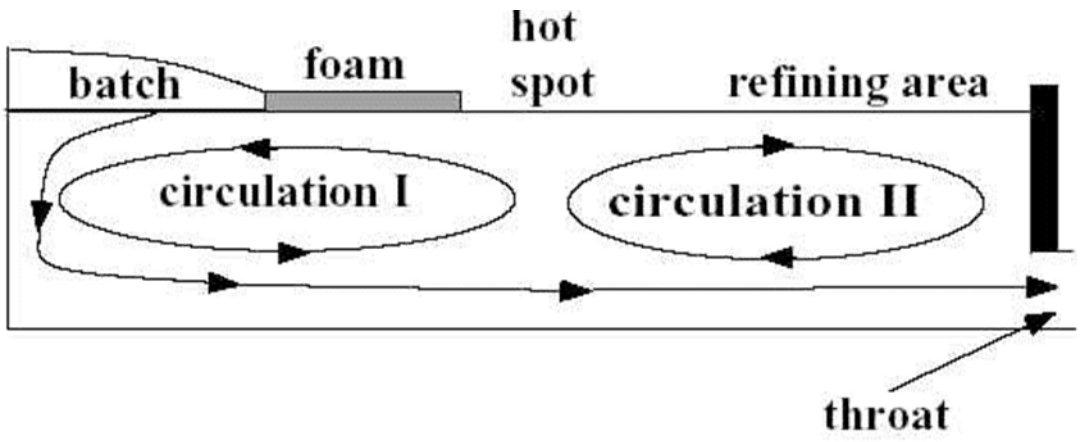

Figure 2.2: Diagram of a glass batch experiment showing thermal convection (Zhigiang and Zhihao, 1997). The two convection cells in this experiment are counter-rotating during the production of glass in a furnace.

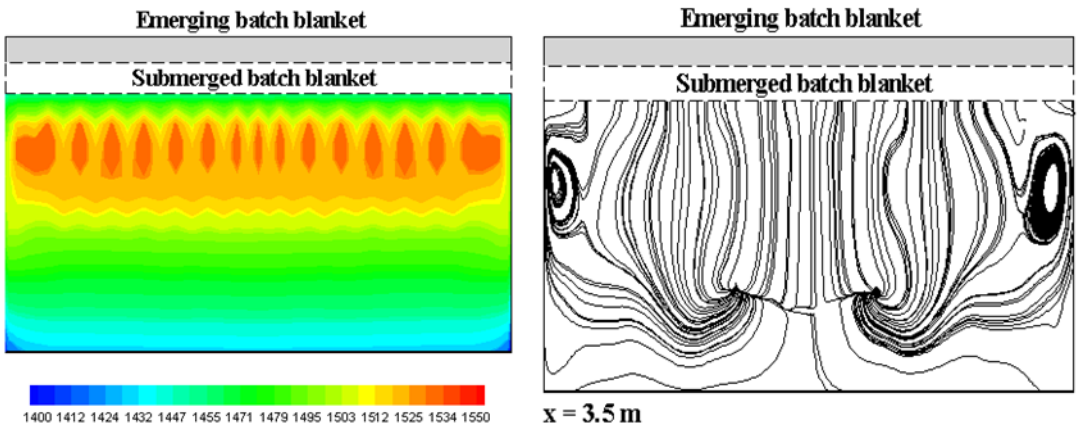

Figure 2.3 a): (above-left) Glass batch image showing the typical fingering pattern resulting from a thermal convection experiment (Pilon et al., 2006). b): (above-right) Glass batch image showing rotation resulting from a thermal convection experiment (Pilon et al., 2006).

Convection in Porous Media

In the late 1940s, it was demonstrated that if a porous-medium layer was heated from below, instability occurs leading to the onset of thermal convection (Horton and Rogers, 1945; Lapwood, 1948). This is of interest not only to geothermal convection study, but also to the problem of contaminant transport stemming from buried nuclear waste.

The onset of thermal convection in a horizontal layer of porous medium uniformly heated from below has been studied in detail using the Horton-Rogers-Lapwood problem (Nield and Bejan, 2006; Nield and Kuznetsov, 2006; Nield and Kuznetsov, 2011). In the case of weak heterogeneity, a Rayleigh number based on the mean properties is an acceptable basis for the prediction of the onset of instability; thus the effects of vertical heterogeneity and horizontal heterogeneity are considered to be comparable (Nield and Kuznetsov, 2006).

Variable density fluid flow occurs in many different forms and localities. When it is caused by solute/colloidal concentration, temperature, and pressure, it can occur in hydrological situations

including seawater intrusion, high-level radioactive waste disposal, groundwater contamination and geothermal energy production (Simmons et al., 2001). Convective currents can arise from heat and salinity gradients acting simultaneously or independently (Angisara and Scrinivasan, 1989). Several studies have shown that density-driven free convection is a likely mechanism for the circulation of large quantities of fluid without the requirement of large external inputs and outputs (Morton and Land, 1987; McKenna and Sharp, 1997; Sharp et al., 2001).

There are various studies which focus on convection in vertical fractures and other conduits. Thermal convection in faulted extensional sedimentary basins has been studied; convection can occur for basal heat flows when the vertical hydraulic conductivity is on the order of 1.5 meters/year and lower (Simms and Garven, 2004). Tracer experiments have shown that buoyancy-induced flow may play an important role in groundwater transport and mixing in open vertical conduits in aquifers (Ronen et al., 1995). Convection in groundwater wells has also been recently investigated. The addition of salt to typical well geometry can further destabilize the already unstable geothermal gradient in the well producing double-diffusive vertical convection (Love et al., 2007). Recent studies in variable density groundwater flow have focused on density-driven free convection, hydraulic gradient-driven forced convection, the porous medium properties and dispersion that reduces density-driven flow (Simmons, 2005). The results of these studies have shown that "only very small to modest density differences (e.g., driven by salinity inversions on the order of several thousand milligrams per liter but often substantially less or by a typical geothermal gradient) are required for free convection phenomena to occur where vertical conduits exist" (Simmons et al., 2008).

Convection Quantification

In controlled settings, convection theory predicts that square or nearly square circulations develop with steady state fingering wavelength that is equal to twice the thickness of the layer in which convection occurs (Diersch and Kolditz, 2001; Van Dam et al., 2009). In simple free convective systems where mechanical dispersion is assumed independent of convective flow velocity, the onset of instability is determined by the value of the Rayleigh number (Ra). This dimensionless number is the ratio between buoyancy driven forces and resisting forces caused by diffusion and dispersion (Simmons et al., 2001). Numerical modeling utilizing the boundary layer Rayleigh number to determine the critical brine thickness necessary for free haline convection to occur, place the Rayleigh number at about 10 (Wooding et al., 1997). Simmons et al., (2001) mentions that a Rayleigh number above a value of 5 may be a potential site for free convection, while pointing out that the larger the Rayleigh number, the more unstable the system.

To estimate how fast a convective fingering pattern may dissipate, convective velocity (U_c) can be found by rearranging the Rayleigh number equation:

$$U_c = \frac{Ra\ D_O}{H}$$

Where U_c = convective speed (meters/second)

Ra = Rayleigh number (dimensionless)

D_O = molecular diffusivity (meters^2/second)

and H = layer thickness (meters)

Thus, if a given layer thickness is 10 meters, with a Rayleigh number of 3.5 x 10^{+05}, the convective speed would be approximately three meters/day. This theory suggests that even if the

layer thickness was as small as 1 meter, convective movement would still occur on the order of decimeters per day (Simmons et al., 2001). In steady state, the free convection problem studied by Horton and Rogers (1945) predicts square convection cells will form with a wavelength equal to twice the layer thickness, while at a pre-steady state the wavelengths will be much higher and have a more narrow circulation (Simmons et al., 2001).

Numerical Convection Models

Numerical models have been developed in order to study groundwater flow and transport affected by three-dimensional thermohaline convection systems. The three-dimensional finite element simulator FEFLOW has been utilized to study two-dimensional and three-dimensional convection problems (Diersch and Kolditz, 1996). Two finite element simulators, HYDROCOIN and ROCKFLOW were also studied using non-linear, coupled, partial differential equations to solve for pressure/hydraulic head, and mass fraction/concentration of the solute component (Kolditz et al., 1996). It was found that a diffusive regime occurs if a stable salinity gradient is heated from below, and a finger regime occurs if hot saline fluid exists on top of a stable temperature gradient. Other models have used a finite volume method (FVM) combined with upwind methods in order to avoid numerical instabilities with varying success (Frolkovic and De Schepper, 2000). The numerical model SUTRA (Saturated and Unsaturated Transport) has also been used specifically to study free convection (Voss, 1984), simulating two-dimensional density dependent groundwater flow and solute transport, while RES2DINV has been used to model resistivity imaging of free convective flows in tanks (Dhu, et al., 2003). This modeling suggests that free convection can be identified in the field with the use of ERI (Van Dam et al., 2009).

Field Evaluation of Convection in Porous Media

In convective theory, heat-driven (thermal convection), density-driven (haline, free and forced convection) are well understood processes and have been extensively investigated in numerical and laboratory experiments. Free convection specifically, is the process of convection driven purely by a density gradient, and has never been directly observed in a field groundwater setting (Simmons and Sharp, 2000). Free, or natural convection is of scientific importance because in comparison with diffusion, it transports a larger quantity, has a significantly lower timescale and enables solutes to spread over much greater distances due to the dimensions of the mixing. Without definitive field evidence, free convection remains an incomplete theory, and an entire class of groundwater problems and issues remain to be explored (Halihan, 2002). Density-driven free convection in groundwater can occur when the density of the invading fluid or plume, is greater than that of the ambient groundwater, and is often produced in the form of fingering patterns or lobe-shaped instabilities. The density stratification resulting from the denser fluid overlying the less dense fluid is the main cause of free convection, and can lead to transport of heat and solutes over larger spatial scales and significantly shorter time scales than compared with diffusion alone (Simmons et al., 2001; Schincariol and Schwartz, 1990). This is especially important when considering the effect of variable density flow in groundwater contamination. When surface-based point source pollution releases heavy leachates into the soil, the higher density contaminants can modify the transport behavior as the plume moves into the groundwater region with an approximate density contrast of 0.35-2.8% between the leachate and the groundwater (Freeze and Cherry 1979, p. 435). The leachate can then sink as it penetrates into the groundwater and is transported not only by forced convection (advection) and diffusion, but also by free convection (Ghebart et al., 1988). Schincariol and Schwarts (1990) demonstrated that plume concentrations of only a few hundred to a few thousand milligrams per liter above

ambient groundwater are sufficient to induce the formation of lobe-shaped anomalies (Schincariol and Schwarts, 1990; Shikaze et al., 1998).

Many problems arise from the fact that convection studied numerically and in the laboratory assume steady-state flow, isotropy and homogeneity. Since the Rayleigh number assumes steady-state, "the Rayleigh number can only provide information concerning onset conditions, and nothing about subsequent temporal development" (Simmons et al., 2001). Heterogeneity is a triggering mechanism for the onset of instabilities, and is also the most important factor controlling whether the instabilities will grow or decay. Long and vertically continuous high-permeability regions (vertical fracturing) tend to enhance growth conditions, while intermediate low-permeability regions provide resistance to horizontal dispersive mixing (Simmons et al., 2001).

The importance of both stable and unstable variable-density groundwater flow and solute transport has been studied in the literature. Seawater intrusion into coastal aquifers occurs when higher density seawater mixes with the lower density freshwater, forming a saltwater front that advances inland (Shikaze et al., 1998) and has been widely studied (Frind, 1982a; Huyakorn et al., 1987; Lee and Cheng, 1974; Pinder and Cooper, 1970; Segol et al., 1975; Segol and Pinder, 1976; Voss and Souza, 1987).

Convection in Fractured and Faulted Systems

Interfracture and intrafracture convection has been recently analyzed in low-permeability shales in the Gulf of Mexico citing fracture spacing, fracture aperture, shale thickness and density gradient as major influences in fluid and solute transport (Simmons et al., 2008). In convection theory, free convection is possible for convection parallel to the fracture plane, perpendicular to the fracture plane and also between fractures, though parallel free convection has been shown to

be the most likely process due to its lower salinity difference requirement for the onset of convection to occur (Simmons et al., 2008). Simmons found that, "the most likely mode of convection in a low-permeability layer is Mode 2B, with free convection occurring parallel to the plane of the fracture" and may occur in most hydrologic settings. Figure 2.4 below shows the three convection modes in a fractured low-permeability layer. "The top figure shows Mode 1 interfracture convection, while the bottom figure shows intrafracture convection perpendicular to the plane of the fracture (Mode 2A) and intrafracture convection parallel to the plane of the fracture (Mode 2B)" (Simmons et al., 2008).

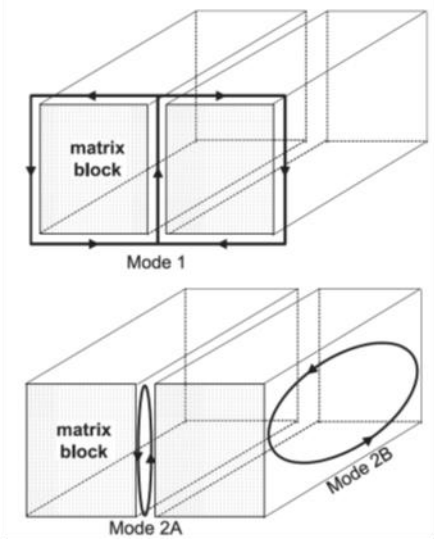

Figure 2.4 a): Diagram of Mode 1 convection cells. b): Diagram of Mode 2A and Mode 2B convection cells (Simmons et al., 2008).

Resistivity and Convection

Electrical resistivity is a geophysical technique which measures the difference in subsurface resistivity utilizing four electrodes. Electrical resistivity methods were first developed in the

early 1900's, though it was not put into use widely until the 1970s (Hauser et al., 1998). More recent developments in in field systems and processing software have produced electrical images which mirror the subsurface more accurately that ever before (Andrews et al., 1995; Reynolds, 1997). These systems use switching between several electrodes to collect a number of resistivity measurements from an array of electrodes. Modern ERI technology has been described as a combination of traditional electrical probing introduced by the Schlumberger brothers, and cutting edge tomography data inversion methods (Daily et al., 2004).

Resistivity is an inherent property of all materials, thus resistivity imaging is well suited for both resistive and conductive materials, and unlike other subsurface methods such as ground penetrating radar (GPR), it functions well under various surface/subsurface conditions and can be used when the field site contains significant topographic variability. The fundamental theory for ERI surveying relies on Ohm's law. Ohm's law describes the relationship between resistance, potential difference and current.

$$R = V/I$$

where R = resistance (ohms)

V = potential difference (volts)

I = current (amps)

The resistance of a wire cable can be expressed as:

$$R = \frac{\rho L}{A}$$

where R = resistance (ohms)

ρ = resistivity (ohm-meters)

L = length (meters)

A = cross sectional area (meters^2)

From this equation, resistivity (ρ) can be defined:

$$\rho = \frac{VA}{IL}$$

where ρ = resistivity (ohm-meters)

V = potential difference (volts)

A = cross-sectional area (meters^2)

I = current (amps)

L = length (meters)

Resistivity (ρ) is the volumetric parameter that defines resistance over a three-dimensional object verses a one-dimensional wire. With the advances in computing power and data logging equipment, resistivity equipment has developed different sampling techniques and different array possibilities. A single survey may contain thousands of data points, allowing for much larger scale, high-resolution surveys.

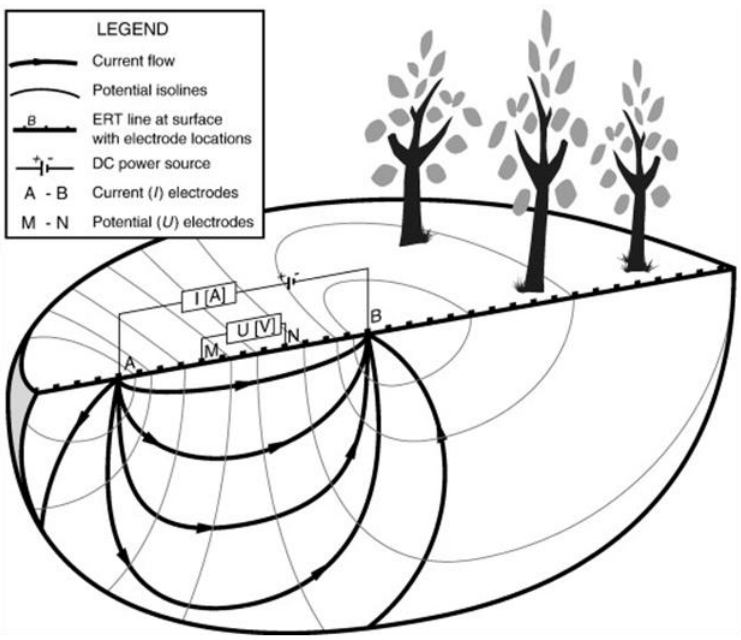

Figure 2.5: Diagram of Electrical Resistivity Imaging technique showing a typical 4 electrode configuration which was used in the field study (Nijland et al., 2010).

Surface resistivity equipment uses a direct current signal (I) which is sent to the electrode array which is connected to the ground surface through metal stakes, while independently measuring different combinations of the potential difference (V) across the electrodes. Power is supplied by dry-cell batteries which can be recharged through the use of portable generators for field work when longer timescales are involved. The process is repeated for several current/potential electrode configurations over a predetermined period of time which allows for the collection and onsite storage of thousands of data points. Data are collected by the ERI equipment over a period of time and is stored in the instrument. Through data inversion processing, ERI can produce two- or three-dimensional subsurface images which allow for an understanding of subsurface resistivity variations tens to hundreds of meters deep for most surveys (Reynolds 1997; Hsu et al., 2010; Smith and Sjogren, 2006). An electrode array with constant spacing is utilized to record changes in apparent resistivity, which then reflects geologic variability or localized subsurface

anomalous features (Wightman et al., 2003). The data gathered by the equipment is interpreted in values of apparent resistivity (ρ_a) and is defined as, "the resistivity of an electrically homogeneous and isotropic half-space that would yield the measured relationship between the applied current and the potential difference for a particular arrangement and spacing of electrodes" (Wightman et al., 2003).

Field-based Detection of Convection in Groundwater

There is a range of evidence that free convective flow of variable-density fluids in groundwater can be detected and monitored through geophysical field techniques. Geoelectrical imaging was conducted in the Okavango Delta, Botswana, to infer the salinity distribution in the subsurface below two islands; one density finger was observed on one of the islands (Bauer et al., 2006). The University of Texas hydrogeology field projects at Padre Island National Seashore included a series of resistivity profiles in tidal flats as well as hydrogeologic mapping which showed an expected freshwater lens overlying saline water from the Gulf of Mexico and the Laguna Madre as well as salinity inversions (UTHFC, 1997, 2001, 2003, 2005, and 2007). A separate resistivity profile conducted in 2000 shows a salinity profile also performed at North Padre Island National Seashore; salinities were inferred from the resistivity profiles and later confirmed with Geoprobe data (Fenstemaker et al., 2001).

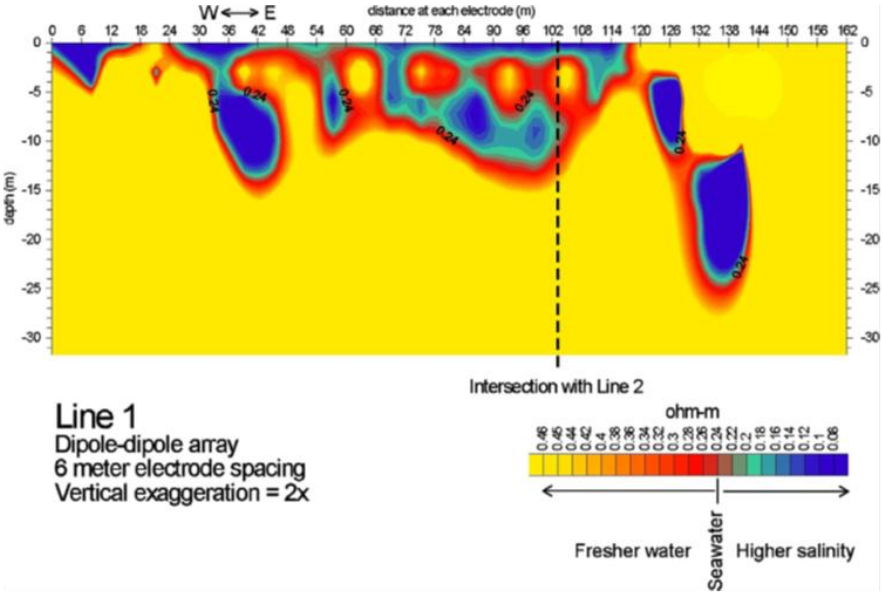

Figure 2.6: Electrical Resistivity Image, North Padre Island, Texas showing unstable density in a field setting (Fenstemaker et al., 2001).

Further investigation at this site by Stevens et al. (2009) included ERI methods along with nested piezometers and data loggers which captured the development of density inversions and plumes of high-salinity water. "Estimated Rayleigh numbers and mixed convection ratios using field data confirmed that inverted density gradients should be unstable", but the existence of free convection at the site was not confirmed by the data (Stevens et al., 2009). The hypothesis, however, that free convection occurs in a natural setting is still considered valid.

In Van Dam et al., (2009), geophysical imaging resulted in a "fingering pattern with lobe structures that descend to variable depths into the aquifer." The pattern found was consistent with fingering patterns found by redissolution of brine. Mode 2B free convective cells were imaged through the use of ERI, though transient and three-dimensional characteristics were not investigated (Van Dam et al., 2009).

CHAPTER III

SITE DESCRIPTION

Geology

The Sierra Nacimiento uplift in northern New Mexico consists of an area over 2,200 km^2 bounded on the west by the San Juan Basin, on the northeast by the Chama Basin, on the east by the Jemez Volcanic Field and on the southeast by the Albuquerque Basin of the Rio Grande rift (Pollock et al., 2004). Mountain building processes and geologic uplift resulted in the structures found there today, and are of importance to many structural geologists who have attempted to interpret the underlying structure of the Sierra Nacimiento. Structures in the Sierra Nacimiento include high-angle reverse faults, thrust faults, steep normal faults, strike-slip faults and north to northwest trending folds (Pollock et al., 2004).

About 75 million years ago, most of the western United States underwent a compressive mountain building event known as the Laramide Orogeny. The Sierra Nacimiento mountain range in New Mexico, was at this time uplifted along a thrust-fault zone on the west side of the mountain range (Woodward, 1987; Woodward and Ruetschilling, 1976). Shear folding of the brittle Precambrian basement rocks occurred, as well as stretching of the incompetent overlying sedimentary strata along a monoclinal fold on the west side of the uplift. The normal faults and folds were cut by the Nacimiento Fault which is close to vertical at depth, flattens upward and

has westward movement of the hanging wall block over the San Juan basin (Woodward et al., 1971).

The Tierra Amarilla anticline is a ridge extending approximately 1,600 meters and includes the Tierra Amarilla mound springs and the Nacimiento Fault. The Tierra Amarilla anticline is located in north-central New Mexico at the junction of several major geologic provinces: the Colorado Plateau, the Rio Grande rift and the southern Rocky Mountains (Woodward, 1987; Cron, 2011). Two major tectonic events resulted in the present day structure of the Tierra Amarilla mound springs site: the Nacimiento uplift during the late Cretaceous and early Tertiary, and the Rio Grande rift during the late Cenozoic. The Tierra Amarilla mounds springs site consists of the "Todilto Formation, Entrada Sandstone (Jurassic), Petrified Forest Member (Triassic), Agua Zarca Sandstone Member (Triassic), and the Glorieta Sandstone and Bernal Formation (Permian), the Abo, and the Yeso, and the Madera (Pennsylvanian) stratigraphic units" (Cron, 2011).

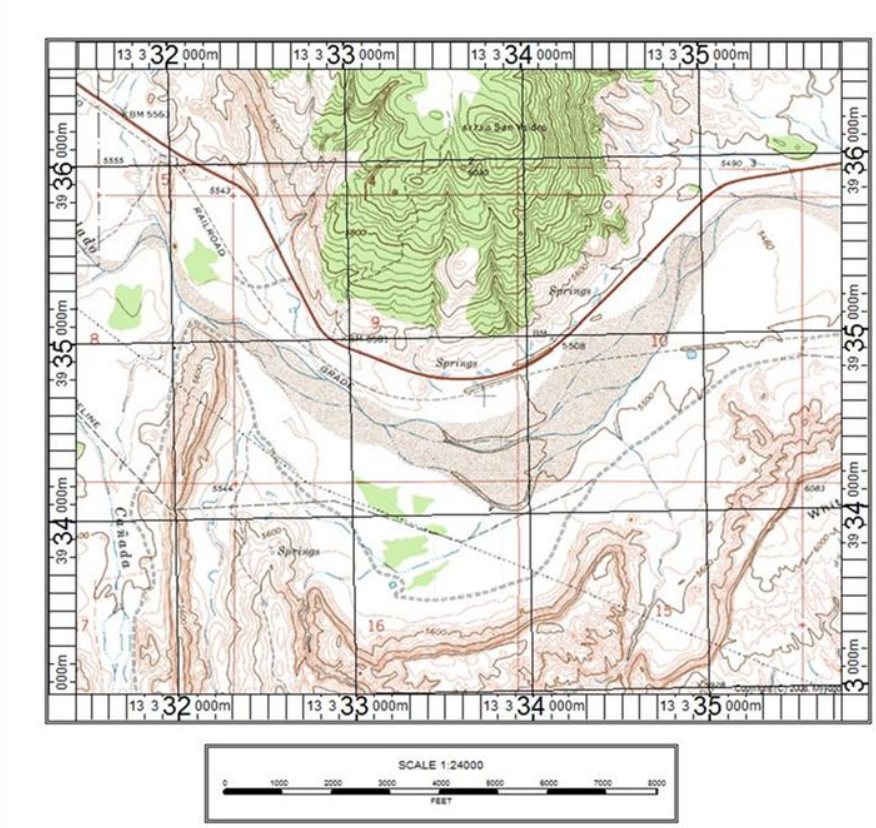

Figure 3.1: Geologic map view of research site (USGS, 2001).

Utilizing the previous work of Cron (2011), two cross sections were created using subsurface structural mapping along with the processed ERI data.

Figure 3.2: Map view showing the positions of the cross sections at research site (aerial photo from Google Earth, May 5, 2012).

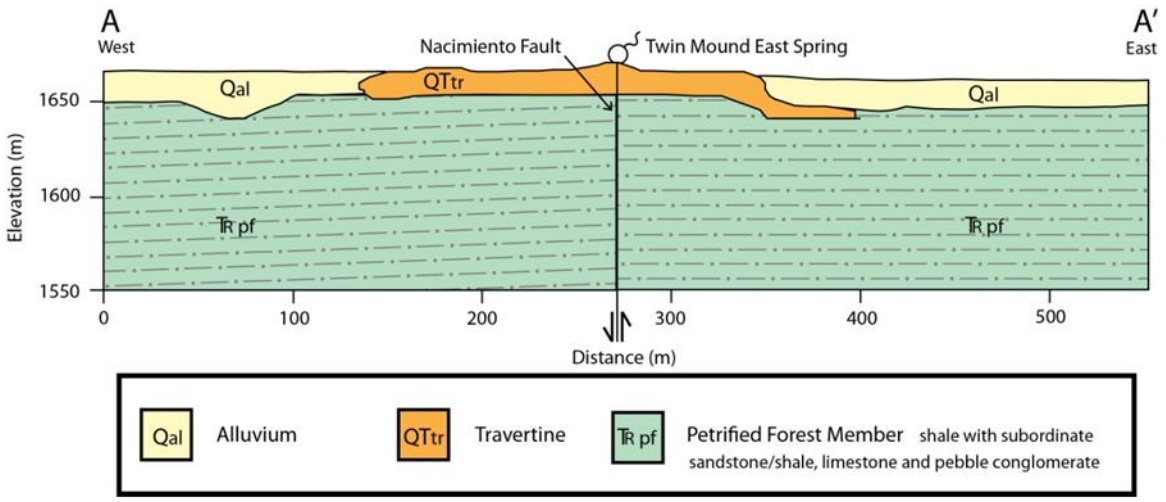

Figure 3.3: Cross section perpendicular to the Nacimiento Fault at Twin Mound East, ERI line EW000.

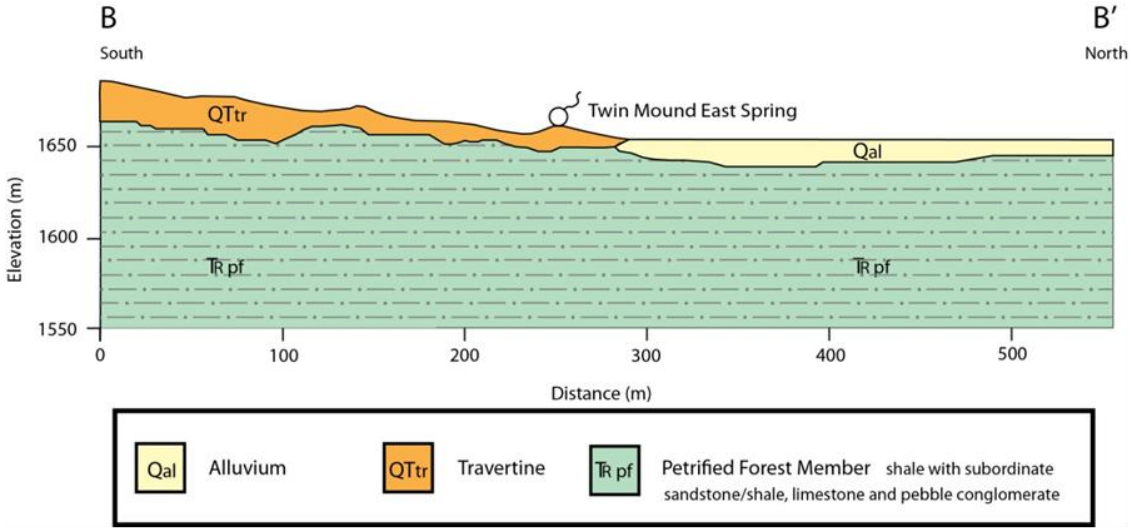

Figure 3.4: Cross section parallel to the Nacimiento Fault at Twin Mound East, ERI line NS000.

Hydrogeology

Helium and carbon isotopic data indicate deep fluid connections in this system. Stable isotope analysis of the study site show that flow from the distal Valles Caldera hydrothermal system may be related to the springs in this area as fluid transport occurs along extensional faults. Travertine continues to be deposited in the area while some extinct mound springs may be as old as 270 ka (Halihan., 2011). The range of TDS in springs at the site has been recorded by Cron (2011), at 4,000-10,000 mg/L. The water chemistry of the study site is generally a sodic water balanced with chloride and sulphate (Figure 3.5).

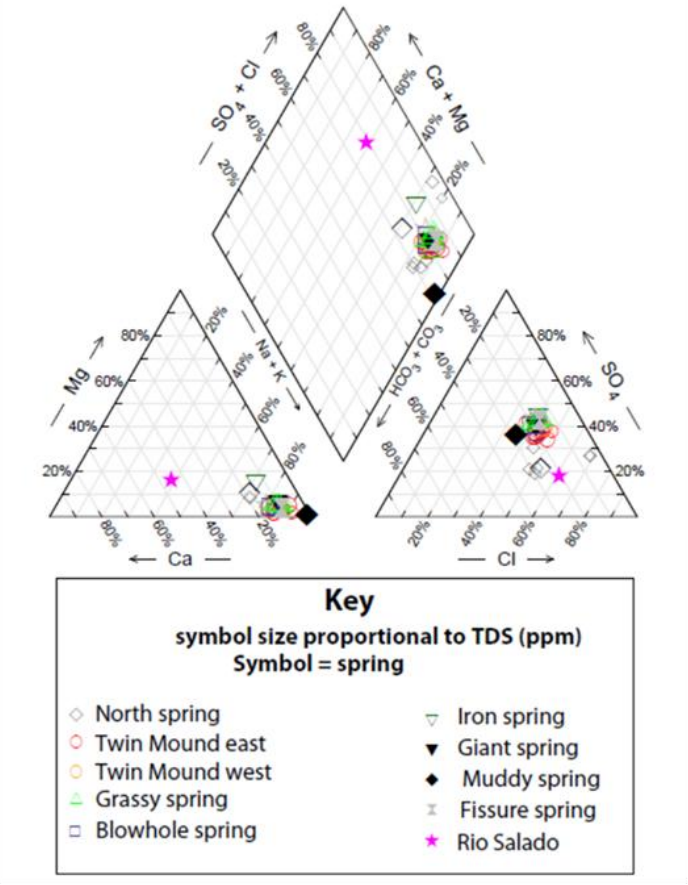

Figure 3.5: Geochemistry of the springs at the Tierra Amarilla mound springs site (Cron, 2011). Twin Mound East spring is included in the geochemical analysis.

The hydraulic gradient parallel to the Nacimiento fault along the Tierra Amarilla anticline was calculated to be 0.08. Generally, fault permeability ranges from 1.00 x 10^{-12} to 1.00 x 10^{-21} meters^2 in faults as found by numerical modeling (Matthai and Roberts, 1999). The permeability (k) of the research site can be approximated upon known values of Petrified Forest shale. Values range from 90-250 Darcies at the Petrified Forest in central Arizona with a porosity of 16-41% (Trendell et al., 2012). Through inspection of geologic maps, the Petrified Forest and the Nacimiento Fault Zone consist of the same formation.

Rayleigh Criteria

The following five Rayleigh number equations are found in Simmons et al., (2008). Mode 1 fracture permeability from the cubic law is $\frac{b^2}{12\lambda}$ where b is the aperture length and λ is the fracture spacing. The average permeability of the medium is:

$$k_{av} = \frac{b^3}{12\lambda}$$

$$k_{av} = \frac{0.005\,m^{\ 3}}{12 * 55\,m}$$

$$k_{av} = 1.89 \times 10^{-10}$$

Mode 1 Rayleigh number equation:

$$Ra = \frac{gk\beta\ Cmax - Cmin\ H}{\theta vD}$$

Where g = acceleration due to gravity (meters/second^2)

k = permeability (meters^2)

β = coefficient of fluid density change ($\partial\rho/\partial C$)

ΔC = concentration difference (dimensionless)

H = layer thickness (meters)

θ = aquifer porosity (dimensionless)

v = fluid kinematic viscosity (meters^2/second)

and D = solute diffusivity (meters^2/second)

$$Ra = \frac{9.81 m/s^2 * 1.00\ x\ 10^{-14} * 0.7 * 0.006 * 60\ m}{0.5 * 1.00\ x\ 10^{-06}\ m^2/s * 1.00\ x\ 10^{-09}\ m^2/s}$$

$$Ra = 49.4$$

The critical concentration difference needed for the onset of Mode 1 convection from the standard Horton-Rogers-Lapwood theory is $4\pi^2$. Thus, an estimate of the critical concentration difference for Mode 1 convection follows (Simmons et al., 2008).

$$\Delta C_{crit} = \frac{48\pi^2 Dav\ v\lambda}{g\beta b^3 H}$$

where π = the constant pi (dimensionless)

Dav = effective diffusion coefficient (meters^2/second)

v = fluid kinematic viscosity (meters^2/second)

λ = effective wavelength (meters)

g = acceleration due to gravity (meters/second^2)

β = coefficient of fluid density change ($\partial\rho/\partial C$)

b = fracture aperture (meters)

and H = layer thickness (meters)

$$\Delta C_{crit} = \frac{48 * (3.14)^2 * 5.00\, x\, 10^{-10}\ m^2/s\ * 1.00\, x\, 10^{-06}\ m^2/s * 55\, m}{9.81\, m/s^2 * 0.7 *\ 0.005\, m\ ^3 * 60\, m}$$

$$\Delta C_{crit} = 2.53 \text{ x } 10^{-07}$$

For Mode 2 convection, the Rayleigh number is based on fluid properties, the vertical gradient, and the half-width of a plane vertical layer (Simmons et al., 2008).

$$Ra = \frac{g\ b/2\ ^4 \beta(\Delta C/H)}{Dav\, v}$$

where g = acceleration due to gravity (meters/second^2)

b = fracture aperture (meters)

β = coefficient of fluid density change ($\partial\rho/\partial C$)

ΔC = concentration difference (dimensionless)

H = layer thickness (meters)

Dav = effective diffusion coefficient (meters^2/second)

and v = kinematic viscosity (meters^2/second)

$$Ra = \frac{9.81 m/s^2 * \left(\frac{0.005\, m}{2}\right)^4 * 0.7 * (0.006/60\, m)}{5.00\, x\, 10^{-10} m^2/s * 1.00\, x\, 10^{-06}\ m^2/s}$$

$$Ra = 53.6$$

Finally, an estimate for the critical concentration difference for the onset of Mode 2A convection follows (Simmons et al., 2008).

$$\Delta C_{\text{crit 2A}} = \frac{500.5\ Dav\ vH}{g\beta b^4}$$

where Dav = effective diffusion coefficient (meters^2/second)

v = fluid kinematic viscosity (meters^2/second)

H = layer thickness (meters)

g = acceleration due to gravity (meters/second^2)

β = coefficient of fluid density change ($\partial\rho/\partial C$)

and b = fracture aperture (meters)

$$\Delta C_{\text{crit 2A}} = \frac{500.5 * 5.00\ x\ 10^{-03} * 1.00\ x\ 10^{-06} * 60\ m}{9.81 m/s^2 * 0.7 * 0.005\ m^4}$$

$$\Delta C_{\text{crit 2A}} = 3.50 \text{ x } 10^{-03}$$

Simmons et al., (2001) states that a Rayleigh number of 5 or above is sufficient to indicate the possibility of free convection, while Wooding et al., (1997) states that a Rayleigh number around 10 is necessary for free haline convection to occur. Nield et al., (2008) states that the

approximate Rayleigh number for the onset of instability would be about 30, slightly less than the value of 40 previously used for the parallel plate problem (Simmons et al., 2008). When the Rayleigh number reaches a value of 40 or above, free convection is assumed to be taking place. Several problems exist with the calculation of the Rayleigh number. Steady-state flow and simple boundary and layer conditions are assumed, a limited knowledge exists for the onset of free convection in a field setting, and spatially distributed properties are averaged for dimensionless computation (Simmons, et al., 2008). The calculated Rayleigh number for Mode 1 free convection was 49.4, while the value for Mode 2 was 53.6; which is above the established theoretical values required for the onset of free convection. The values calculated here indicate the probability of free convection exists as Mode 1 and Mode 2 Rayleigh numbers are both above 40, while keeping in mind that the Rayleigh number is only an indicator of instability and does not have the ability to prove free convection in the field.

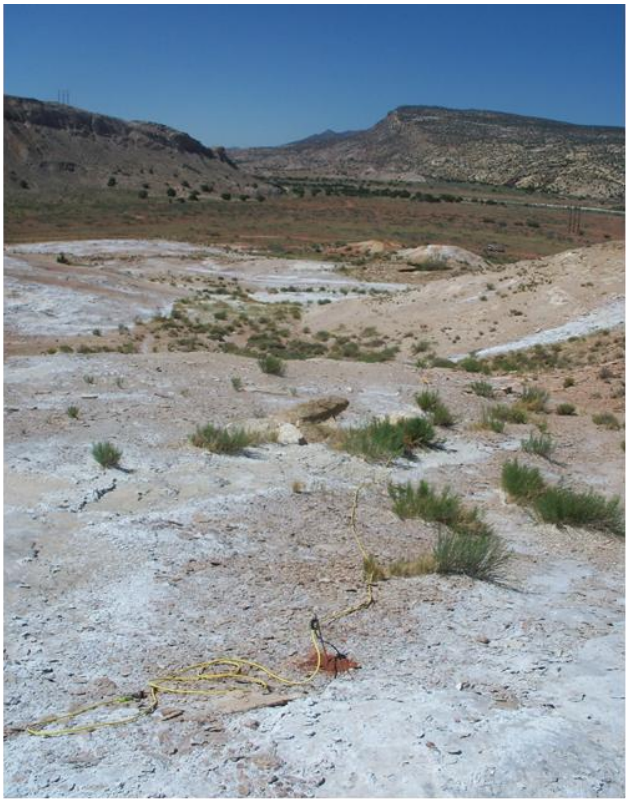

Figure 3.6: Photo of the NS000 transient ERI line facing north, parallel to the Nacimiento Fault.

Figure 3.7: Photo of a seeping spring at the Tierra Amarilla mound springs site.

Figure 3.8: Photo of the Nacimiento Fault facing north. Photograph taken from a few hundred meters south of the study site.

CHAPTER IV

METHODS

In May of 2011, a team from Oklahoma State University in coordination with the University of New Mexico used ERI in order to investigate the possibility of free convection at the Tierra Amarilla mound springs site. Six ERI data sets were collected along the length of the fault and also perpendicular to the fault (Figure 4.2). Based on the preliminary data, twelve additional ERI datasets were collected in a pseudo three-dimensional array the following year. The field methods employed at the site included GPS surveying, water quality sampling and monitoring, ERI data collection, and geologic mapping. The analysis of the data included data reduction and processing of the above methods and a wavelength analysis of the electrical resistivity data.

Resistivity Design

The ERI equipment used at the Tierra Amarilla mound springs site consists of an Advanced Geosciences, Inc. *SuperSting R8* multi-channel portable earth resistivity meter, a switchbox which connects the main unit and the electrodes, cable with 56 electrodes spaced every 10 meters, and one stainless steel stake for each of the 56 electrodes. The ERI unit's power supply was derived from several 12-volt marine deep cycle batteries that had the ability to be recharged.

Using the preliminary data from May 2011 as a guide (Figure 4.2), a pseudo three-dimensional survey was designed in order to plot the data points that would be required in the field.

Figure 4.1: Map view of the Nacimiento Fault; dashed line indicates an inferred fault (aerial photo from Google Earth, May 5, 2012).

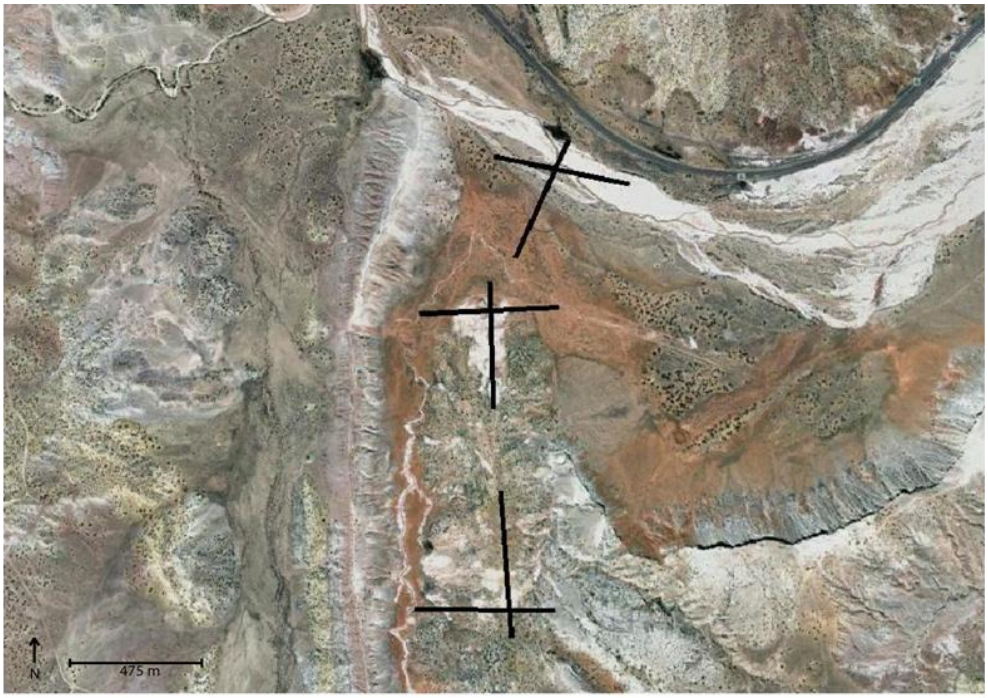

Figure 4.2: Map view of preliminary ERI survey lines collected during May, 2011 (aerial photo from Google Earth, May 5, 2012).

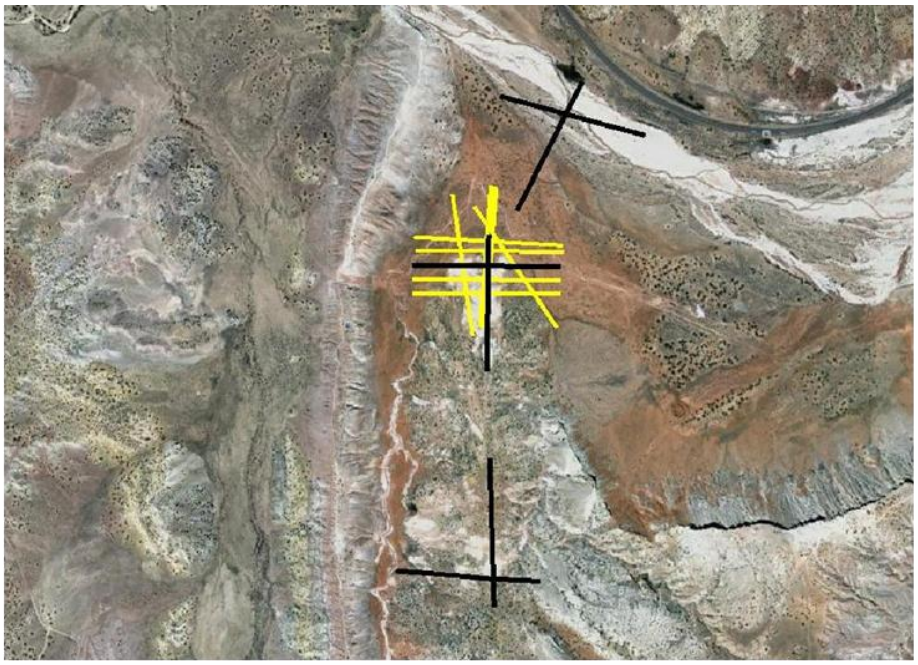

Figure 4.3: Map view of ERI survey lines plotted from GPS data; June, 2012 shown in yellow. Preliminary data from May of 2011 shown in black (aerial photo from Google Earth, May 5, 2012).

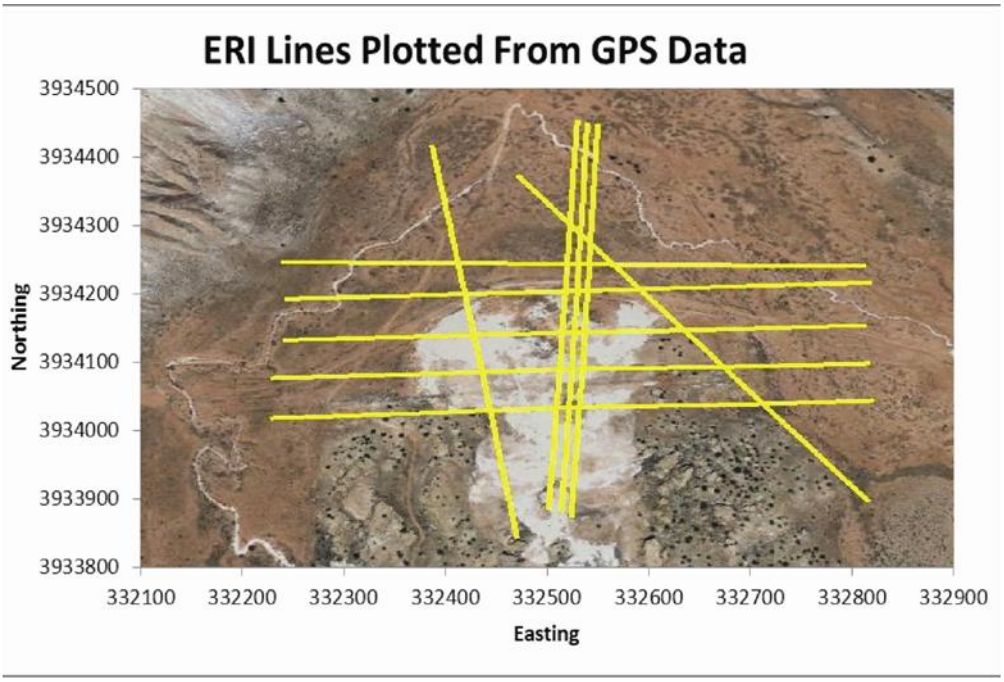

Figure 4.4: Pseudo three-dimensional ERI survey lines plotted from GPS data with easting and northing coordinates (aerial photo from Google Earth, May 5, 2012).

Figures 4.1-4.4 demonstrate that the pseudo three-dimensional ERI survey design was concentrated along the strike of the Nacimiento Fault in order to capture Mode 2A and Mode 2B convective cells, along with Mode 1 convective cells orthogonal to the Nacimiento Fault. The 2012 survey was designed so that ten ERI lines were to be collected; five running in an east-west orientation, three lines in a general north-south orientation along the fault zone, two lines placed in diagonal orientations, and two more transient datasets to be collected from the central north-south oriented ERI line. Each line consisted of 56 electrodes at 10 meter spacing between each electrode for a total length of 550 meters. The lines were named based on their general orientation and distance from the center point of the survey (Twin Mound East). The central north-south line located directly over several springs was used to observe transient electrical changes in the conductive features which can be interpreted as Mode 2B convection cell rotation.

At the intersection of the central north-south ERI line (NS000) and the central east-west ERI line (EW000), lies the active mound spring Twin Mound East. The NS000 ERI line was imaged at 3 day intervals a total of three times in order to collect transient data which would evaluate the possibility of convection in a weekly timescale. The EW000 line was recollected at the same location and orientation from the previous year providing an evaluation of Mode 1 transient behavior on an annual timescale.

Field Surveying

Springs located along ERI lines were the focus of fluid data collection. A handheld EC meter was utilized in order to collect fluid data at Twin Mound East. A data logger was also used at the site to record the barometric pressure, water level, temperature and conductivity of the fluid inside Twin Mound East at the intersection of lines EW000 and NS000 over a timescale of 24 hours.

Differential GPS, a laser range finder, and a handheld GPS unit were used to map the topography of the site. After the flagged survey stakes were placed in their pre-selected positions to mark the orientation of each line, 100 meter measuring tapes were used to determine the electrode locations. Then, 56 (50 cm long) stainless steel stakes were driven into the travertine and soil using sledgehammers. After all 56 stake-electrode connections were secured and connected to the resistivity instrument cables and all connections were visually verified, the unit was powered on and stake-electrode connectivity was tested for contact resistance. Due to the highly resistive nature of the travertine along with the dry surface conditions, several stakes had a slurry mixture added around them, composed of native soil and saline fluid extracted from Twin Mound East. After a successful contact resistance test, the *SuperSting R8* unit was allowed to automatically collect data.

In order to image Mode 1 convection cells, ERI line EW000 was placed at the same coordinates in May of 2011 and June of 2012. ERI line NS000 was also placed at the same coordinates and imaged a total of three times during 2012 in an attempt to image Mode 2B convection cells. The stakes for line NS000 were deployed for 6 days and not moved between dataset collection.

Data Analysis

The *Superting R8* (Advanced Geosciences Inc., Austin, TX) system utilizes a menu based program to induce DC current, measure the resulting potentials and store the data for later processing (Halihan et al., 2011). The data collected by the Advanced Geoscience's Inc. *SuperSting R8* was stored in the unit on site, downloaded through the use of a laptop and later processed using a series of software programs. Utilizing the Halihan-Fenstemaker technique, two-dimensional color models were produced which show the distribution of electrical resistivity gathered by the unit in the field (Halihan and Fenstemaker 2004). The two-dimensional images were further processed into a three-dimensional model for further analysis.

The size of potential convection cells were quantified by analysis of the wavelengths of electrical features using the Rose criterion for signal-to-noise. Signal-to-noise ratio is a statistical measure which compares the level of a specific signal to the level of background noise and can be applied to any form of signal (Barker, 1990). In the context of experimentation, a value that is significantly away from zero defines a signal in contrast to noise. The Rose criterion states that a signal-to-noise ratio of at least 5 is needed to distinguish image features as statistically likely. The method was employed by extracting a horizontal line of resistivity data at the elevation of circular conductive anomalies, which generally occurred at a depth of approximately 40 meters in the resistivity datasets. A lower threshold of 2 ohm-meters was used to define conductive features. The size of the features was measured to determine the wavelength of all conductive

features at the horizon utilized. The wavelengths were then compared by dividing the average wavelength by the standard deviation of each ERI line and graphing the results. This method estimates the location of a Mode 1 or Mode 2B convection cell, but it is an upper bound estimate of the width of the cell. Additionally, for datasets with a limited number of cells, the statistical method is applied to a small number of samples, but still provides a reliable method independent of observer.

CHAPTER V

RESULTS

After the preliminary survey of six resistivity datasets, a total of ten ERI survey lines were imaged in June 2012, at the Tierra Amarilla mound springs site in north-central New Mexico, using the AGI equipment previously described (with an additional two transient lines imaged). The ERI line along the Nacimiento Fault (NS000), was collected three times in order to evaluate the transient properties of Mode 2B convective cells. The results are presented based on the fluid data collected and the relationship between fluid and resistivity data first. Next, the resistivity data and the wavelength analysis are presented. Finally, the transient data from the Mode 1 and Mode 2B collection efforts are presented.

Fluid Results

The fluid data obtained from the site include conductivity, water level, air pressure and temperature at the central travertine-depositing mound spring Twin Mound East. Conductivity at the mound spring over a timescale of 24 hours was shown to have significant salinity fluctuations while the barometrically-compensated level of the spring is steady (Figure 5.2). The temperature of the spring was found to be a constant 24.7^0 C for the duration of the 24 hour timescale measured from June 19-20, 2012 (Figure 5.3).

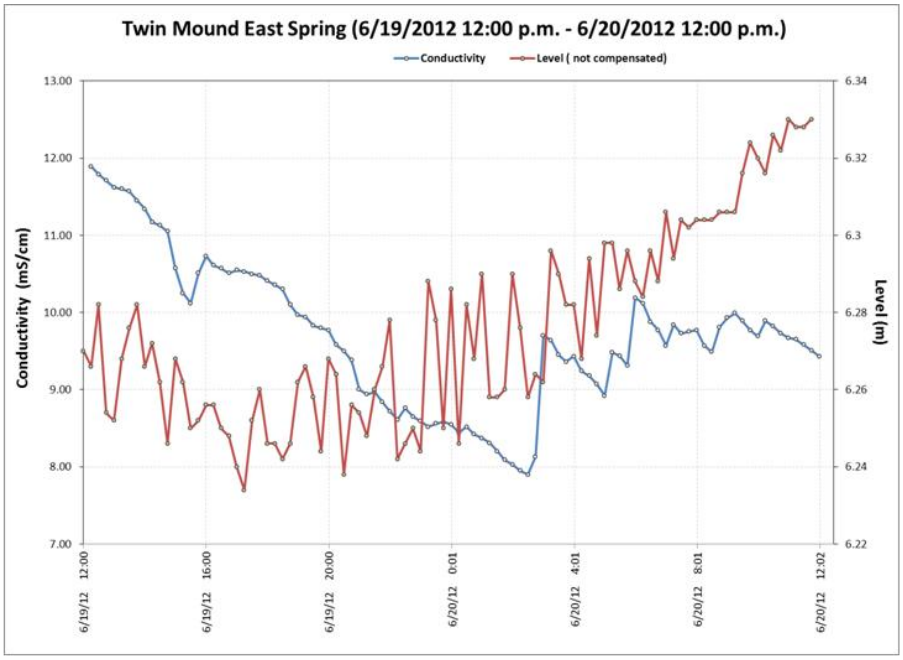

Figure 5.1: Conductivity and water level at Twin Mound East spring over a 24 hour timescale, June 19-20, 2012.

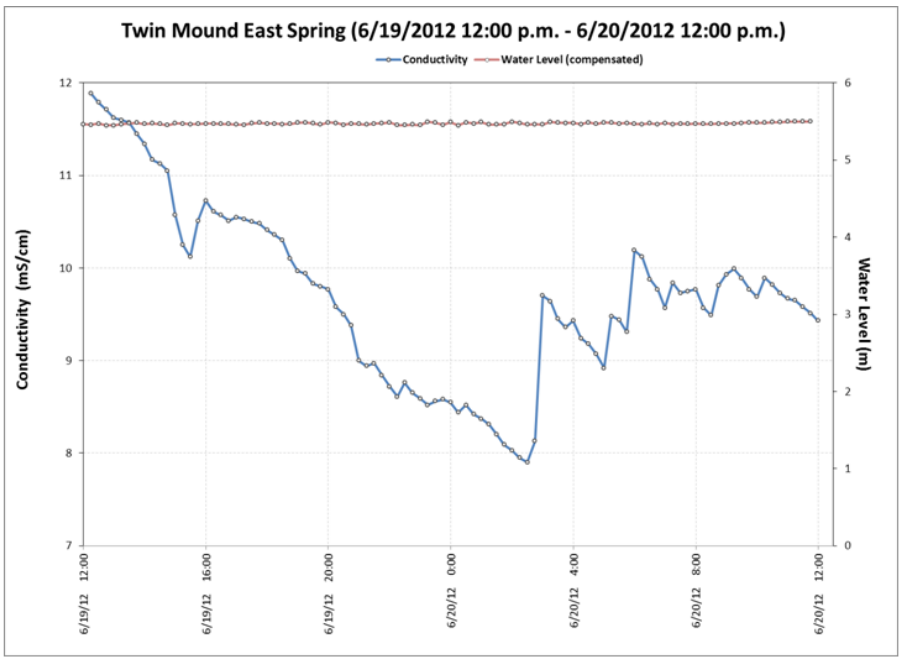

Figure 5.2: Conductivity and barometrically-compensated water level at Twin Mound East spring over a 24 hour timescale, June 19-20, 2012.

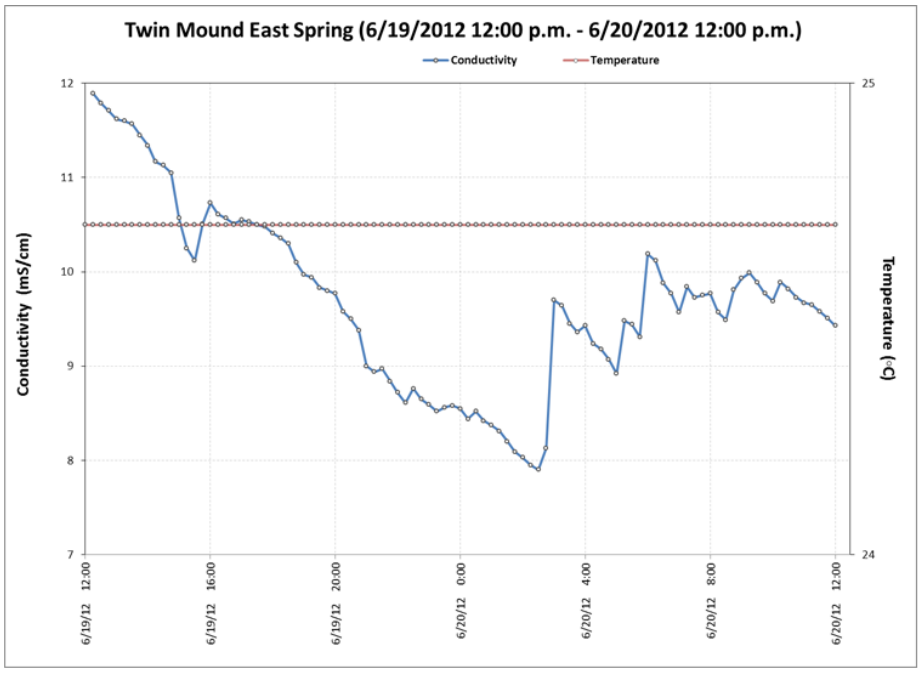

Figure 5.3: Conductivity and temperature at Twin Mound East spring over a 24 hour timescale, June 19-20, 2012.

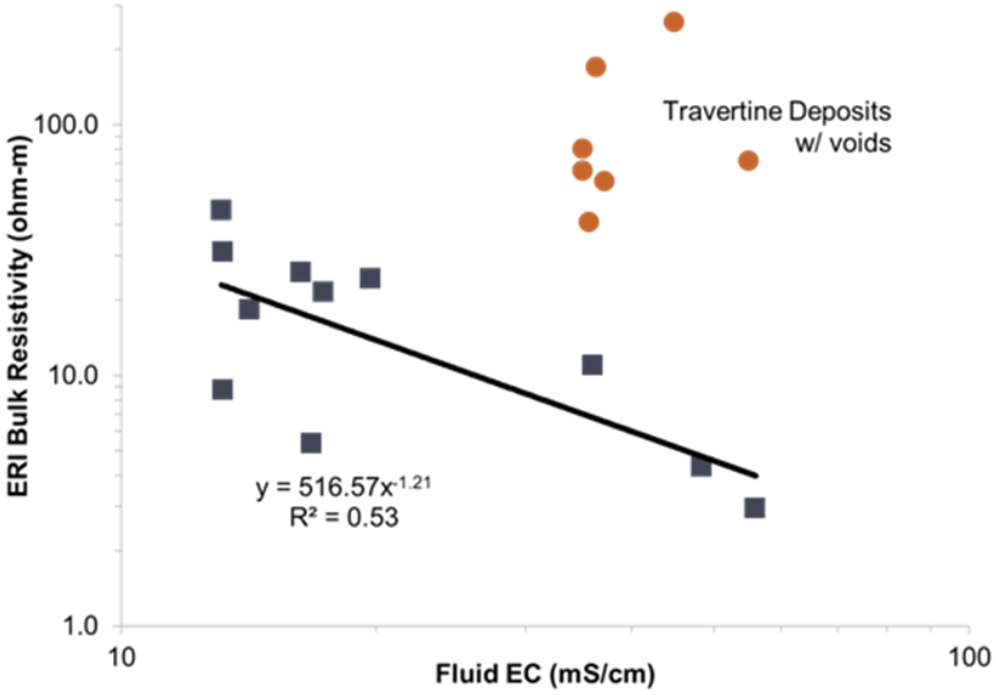

Figure 5.4: Fluid conductivity and bulk electrical resistivity correlations from May, 2011.

The electrical conductivity (EC) of the springs is related to the bulk resistivity of the springs when the resistivity is below approximately 30 ohm-meters (Figure 5.4). The higher resistivity areas do not show a relationship. The relationship between the measured EC values for the springs at the site and the bulk resistivity of the springs is affected by the structure of the travertine deposits. In areas where the springs are discharging from travertine which is loosely attached to the underlying formations, the bulk resistivity is higher and the travertine sounds hollow when walking upon it, or driving a metallic stake into it with a sledgehammer. In other areas the travertine appears competent and the relationship is much stronger.

Resistivity Results

Results from the ERI data gathered and processed are presented below. The preliminary results from 2011 are presented followed by the results of wavelength analysis of the 2012 datasets. Finally, the results of the transient evaluation of potential Mode 1 and Mode 2B convective cells are presented.

ERI Preliminary Data

Preliminary data showed conductive circular features in both Mode 1 cell configuration (perpendicular to the fault) as well as Mode 2B configurations along the fault (Figure 5.5). Orthogonal to the fault, a resistive signature with an approximately 55 meter width is present along the fault with a resistivity range of 5-10 ohm-meters. Resistive areas greater than 30 ohm-meters are located near the surface and correspond to areas with significant travertine deposits (Figures 3.3 and 3.4). Orthogonal to the fault are two conductive features which appear to curl

antithetical to the fault at a depth of approximately 40 meters below the surface. In the fault plane, a number of conductive circular features are observed near the same depth interval.

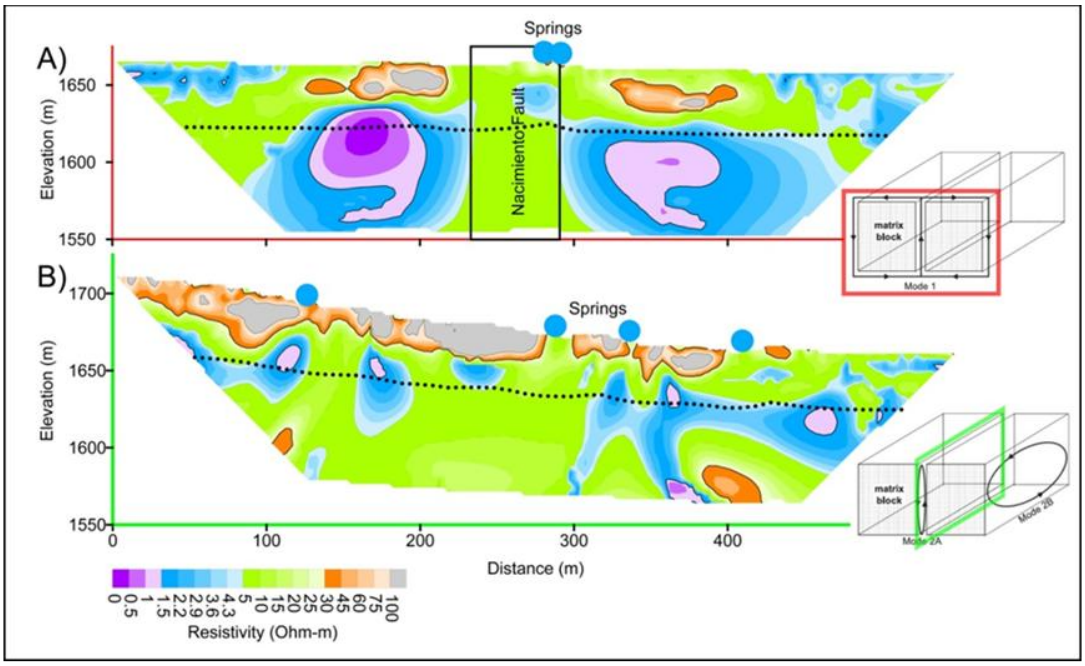

Figure 5.5: ERI images of TAM001 (upper image) and TAM002 (lower image) from the Tierra Amarilla mound springs site, May 2011, and their corresponding hypothesized convection cell diagrams. Dashed lines indicate the 40 meter depth surface that was evaluated for wavelengths.

Three-Dimensional Evaluation

Resistivity data from 2012 created a pseudo three-dimensional dataset that was evaluated for wavelengths of potential convection cells (Figure 5.6). The three-dimensional data show more resistive areas corresponding to the location of travertine deposits near the surface. The more conductive areas near the surface corresponding to alluvial deposits or exposures of the Petrified

Forest shale. In the subsurface, conductive circular features are present along the fault plane and in two lines parallel to the fault approximately 100 meters on either side of the fault.

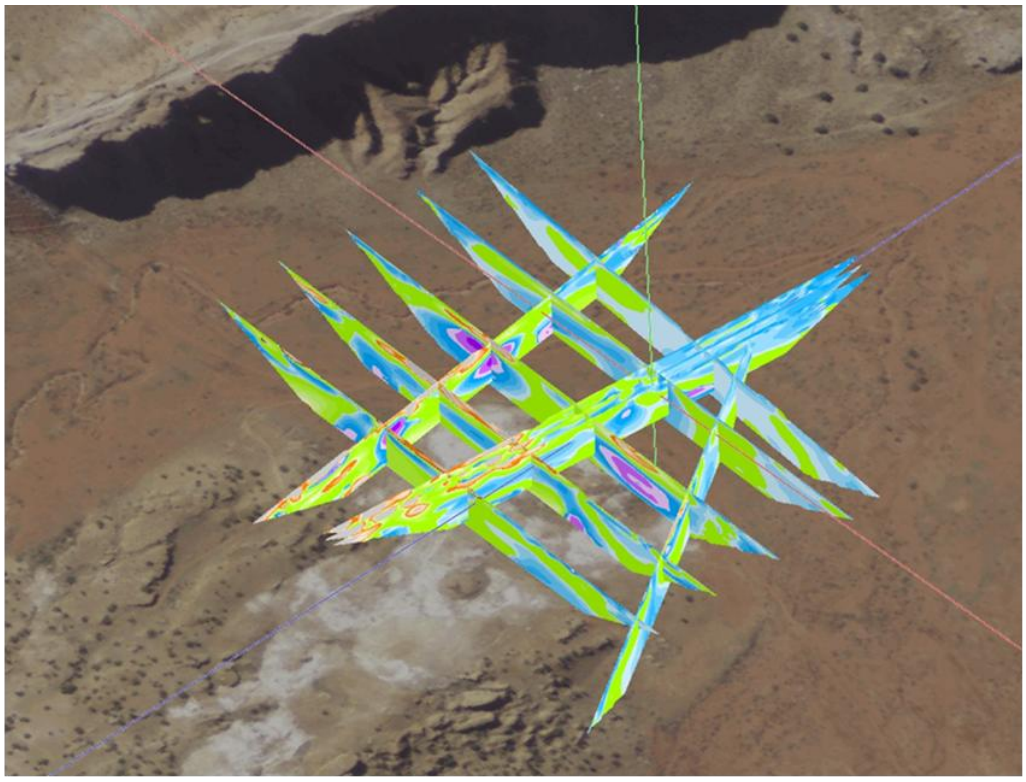

Figure 5.6: Three-dimensional Rockworks image created from the ten ERI lines collected over the Nacimiento Fault, and placed over an aerial Google Earth satellite image taken May 5, 2012.

Wavelength Evaluation

Shown in Figure 5.7, the Rose criterion was used to analyze the wavelengths of the convective cells. This method was successful in predicting where a convective cell would exist, but is an upper bound estimate of the width of the cell. A signal-to-noise ratio value of 5 or above is necessary to distinguish a signal from background noise at a statistical certainty.

Potential Mode 2B convection cells were expected along the fault and Mode 1 convection cells were expected orthogonal to the fault. In other areas where ERI data were collected, no cells were expected. Examples of images with various wavelengths and Rose criteria values were generated in the analysis. The ERI line EW000 was expected to have the ability to image Mode 1 convection cell features based on preliminary work. The measured average wavelength for ERI line EW000, was 195 meters with two possible convective cells present and a Rose criteria value of 14 (Figure 5.7). ERI line NS000 was also expected to image Mode 2B convective cells as it was aligned with the Nacimiento Fault. The convective cell features obtained resulted in an average wavelength of 128 meters for three expected convective cells with a Rose criteria value of 16-17.5. ERI line NSP010 potentially had observable Mode 2B cells as it was 10 meters off of the centerline of the fault. The measured wavelength of conductive features was 86 meters for four cells with a Rose criteria value of 4. Finally, ERI line EWP100 was not expected to have convection cells, and the analysis yielded no cells and was assigned a Rose criteria value of 0.

In total, six ERI lines were expected to have Mode 1 or Mode 2B convective cells have a Rose criteria value of 11-18 (Figure 5.7). The Mode 1 wavelength estimate was 110 meters. Mode 2B wavelength estimates ranged from 110-128 meters. Most lines that potentially contained convective cells had a smaller Rose criteria ranging from 2-9. The wavelength estimate for Mode 1 convective cells was 65-195 meters, and for Mode 2B cells, it was 110-197 meters. Finally, none of the lines that were not expected to have cells had Rose criteria exceeding a value of 1.

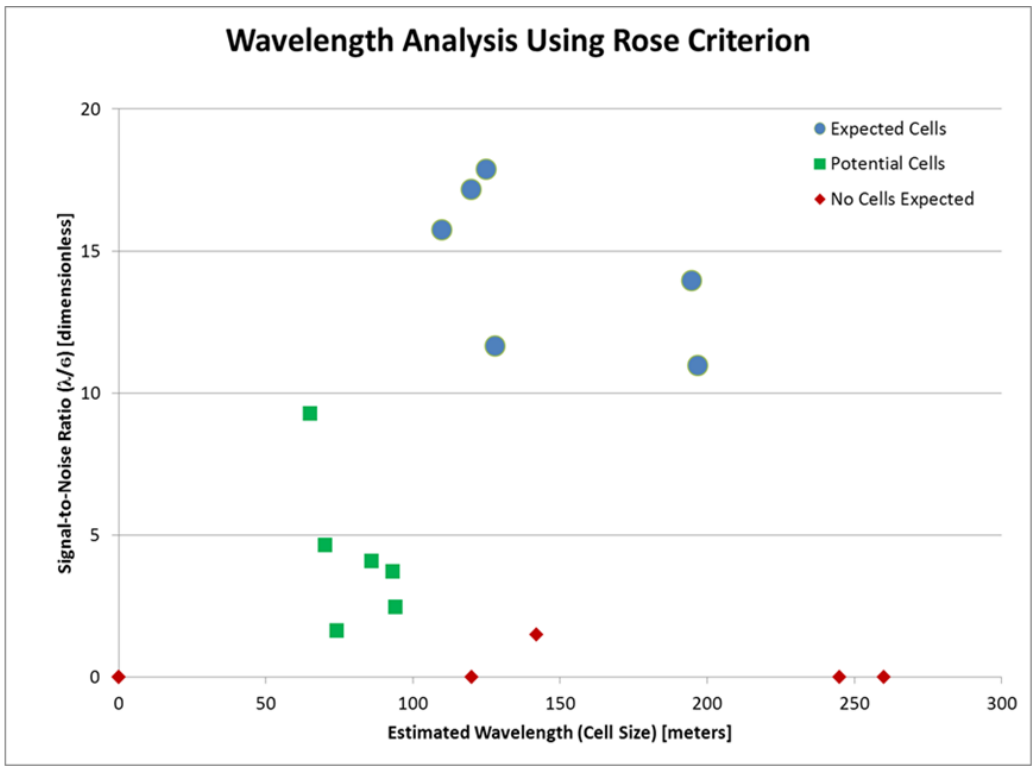

Figure 5.7: Wavelength analysis using the Rose criterion showing expected cells, potential cells, and no cells expected. A Rose criteria value above 5 indicates that a signal exists.

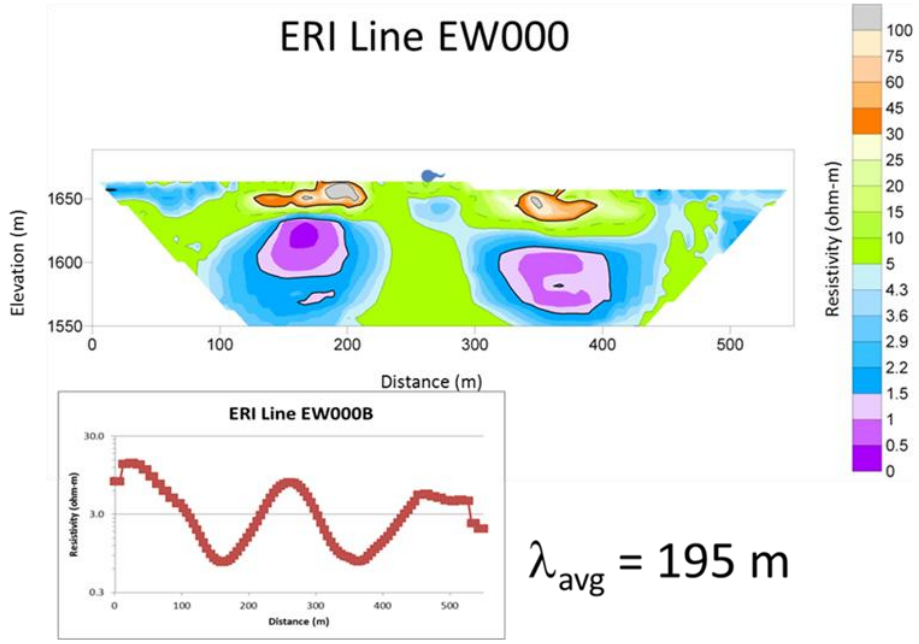

Figure 5.8: ERI line EW000 showing highly conductive antithetical pinwheels on either side of the Nacimiento Fault with an average wavelength of 195 meters. The two expected cells give a Rose criteria value of 14. Graph indicates resistivity data from a depth of 40 meters in the dataset.

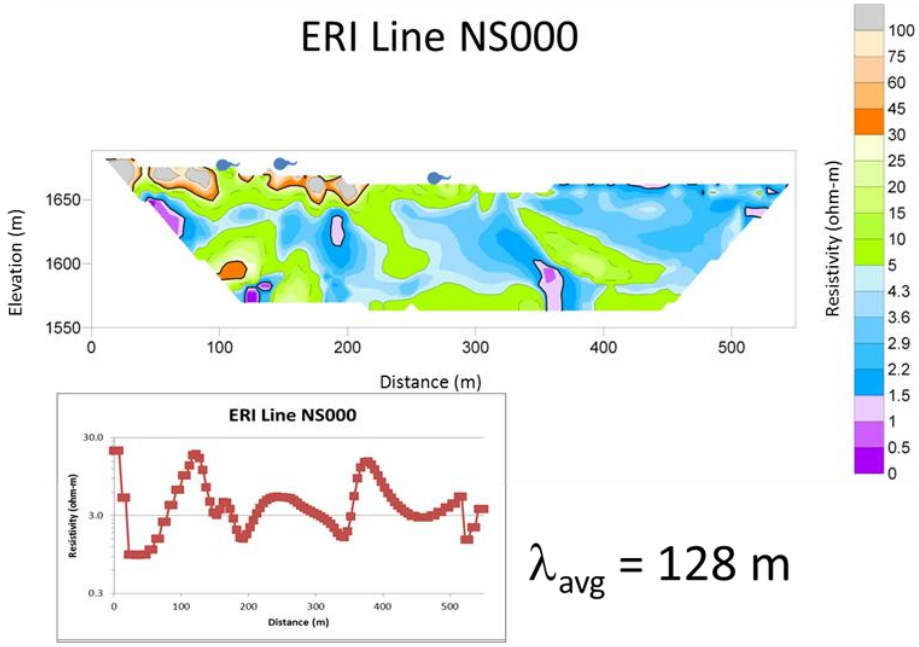

Figure 5.9: ERI line NS000 with Mode 2B convective cells expected as determined by the Rose criterion. Average wavelength was determined to be 128 meters with a Rose criteria value of 12. Graph indicates resistivity data from a depth of 32 meters in the dataset.

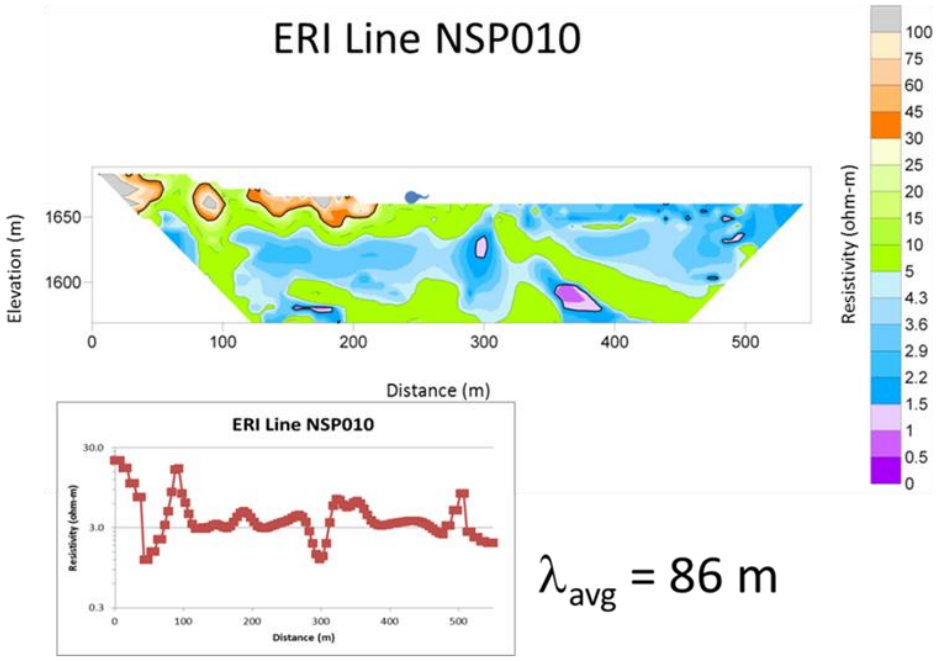

Figure 5.10 ERI line NSP010 with potential convective cells expected as determined by the Rose criterion. Average wavelength was determined to be 86 meters with a Rose criteria value of 4. Graph indicates resistivity data from a depth of 38 meters in the dataset.

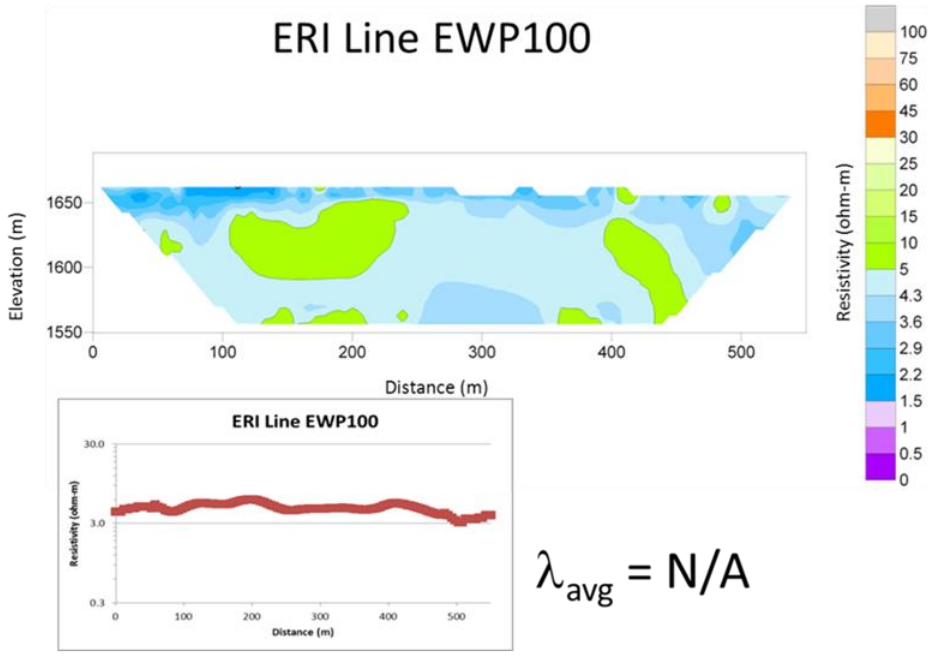

Figure 5.11: ERI line EWP100 with no convective cells expected as determined by the Rose criterion. Average wavelength is not applicable. Rose criteria is assumed to be a value of 0. Graph indicates resistivity data from a depth of 38 meters in the dataset.

Transient Data

The transient data for possible Mode 1 cells was available from a line orthogonal to the Nacimiento Fault through Twin Mound East spring (Figure 5.9). The data were collected 1 year apart and the stakes were not left in place, so the data are evaluated to determine general repeatability. Both datasets showed a similar resistivity pattern with a resistive fault zone between 5-10 ohm-meters with resistive travertine in the shallow central portion of the domain. During both years, antithetical conductive features were present on each side of the fault centered approximately 100 meters from the center of the fault (Figure 5.12). While the general pattern of the conductors remained similar between the two datasets, the structure was somewhat different.

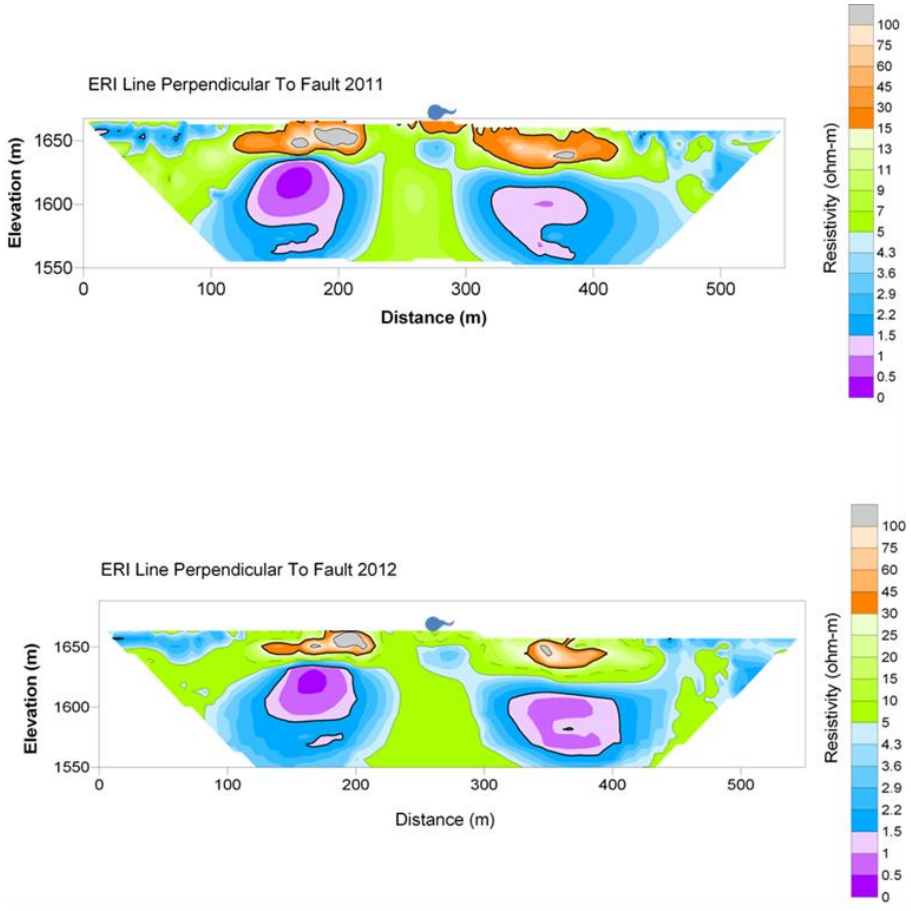

Figure 5.12): Transient resistivity images showing Mode 1 interfracture convection signatures from the central east-west ERI line, perpendicular to the Nacimiento Fault. a): shows data collected and processed in May 2011 (ERI line TAM002), while b): shows data collected and processed in June 2012 (ERI line EW000).

Transient data along the fault was collected on 3 day intervals along the fault on line NS000 (Figure 5.13) to evaluate potential Mode 2B cells. Each interval demonstrated positive and negative changes in resistivity. The data changes over the 6 day interval range from a nearly 50% decrease in bulk conductivity to an increase in conductivity of approximately 60%. The changes in resistivity occur at two distinct intervals vertically with one set of changes occurring approximately 15 meters below land surface and 40 meters below land surface.

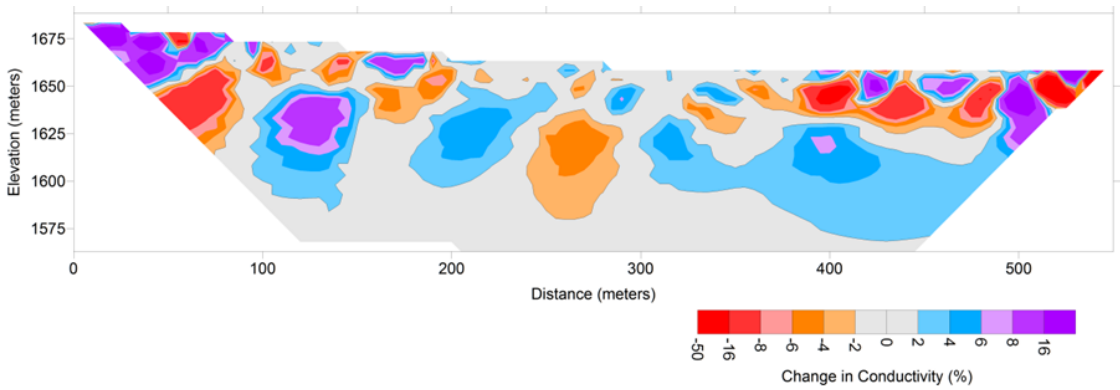

Figure 5.13: Transient resistivity data showing change in bulk conductivity of up to 60% over a 6 day period for ERI line NS000 located directly over the Nacimiento Fault. Circular regions of resistivity changes occur at both 15 and 50 meters below land surface.

CHAPTER VI

DISCUSSION

The primary purpose of this field research was to provide the first quantification of free convection in a hydraulically active fault zone. The hypothesis of this study maintains that free groundwater convection exists at the Tierra Amarilla mound springs in the Nacimiento Fault Zone, and can be quantified through the use of electrical resistivity and transducer data.

What is Required to Prove Free Convection in the Field?

Three criteria must be met in order to demonstrate that free convection is a mechanism for fluid flow in a natural setting. 1 – Lack of alternative diffusive mechanism: field data must demonstrate that flow and transport cannot be generated through diffusion; time scales must be shorter and length scales must be longer. 2 – Lack of ambient field gradients to support advection: the hydraulic gradients must be low enough to not support forced advection as a mechanism to explain the observed flow field. 3 – Direct field verification: field data must support techniques which would infer free convection from physical or numerical experiments, and buoyancy calculations must provide a theoretical basis for the invocation of free convection as the mechanism for flow. Flow field observations must demonstrate either upward movement of dense solutes or full flow circulation field (free convection cell). A corrugated flow field or

fingering must be demonstrated having large density contrasts in horizontal and/or vertical directions (Halihan, 2002).

Data from the Nacimiento Fault

Data gathered from the field site in May 2011 show that there is a relationship between ERI resistivity and fluid electrical conductivity (Halihan, 2011). The fluid upwelling along the fault plane included a primary zone of about 55 meters wide orthogonal to the strike of the fault, and appeared to interact with adjacent aquifer materials (Figure 5.5). An average conductive wavelength of 70 meters was recorded for Mode 2B equidimensional cells along the strike. Orthogonally, the cells were shown to have an average wavelength of 197 meters for Mode 1 cells and are antithetical. Data gathered in June 2012 further demonstrates the relationship between electrical resistivity and conductivity at the site. The average conductive wavelength in 2012 was found to be 128 meters for Mode 2B equidimensional cells along the strike, while the orthogonal Mode 1 cells had an average wavelength of 195 meters. The 2011 data shows more defined Mode 2B cells verses 2012, while the Mode 1 cells are similar in shape and wavelength.

A total of 16 ERI lines were imaged in the Tierra Amarilla mound springs site in north-central New Mexico approximately 80 kilometers northwest of Albuquerque. Two additional images consisting of the transient line NS000 surveyed along the Nacimiento Fault at 3 day intervals. The ERI images show highly conductive cells and fingering patterns associated with free convection in the fault and also perpendicular to the fault. The three-dimensional image created from the data shows that the highly conductive cells are circular in shape and are contained within the Nacimiento Fault Zone. The high topographical gradient causes the two main circular conductive features to break apart as they travel downwards in elevation towards the north. The analysis of the wavelengths was completed through the application of the Rose criterion. The

signal-to-noise ratio was successful in predicting where the expected convective cells existed. All of the expected convection cells have a signal-to-noise ratio above a value of 10, well above the value of 5 which is needed to indicate a signal.

Disproving Possible Anomalies Other Than Free Convection

Fault asperities do not explain the abnormally high conductive features shown in the ERI data, or allow for values of below 5 ohm-meters. Asperities also do not explain a symmetrically spaced electrically conductive feature. In order from least to most likely, proposed explanations of the recorded data which could also result in the processed ERI images obtained include:

1 – Conductive lithology consisting of clays and/or metallic deposits in two circular shapes on opposite sides of the fault.

2 – Fluid-filled voids consisting of two caves formed by travertine that mirror each other on either side of the fault.

3 – Fluid upwelling of two fluids with a conductive gradient.

4 – Haline free convection underneath the travertine mound spring in an antithetical corkscrew motion.

Conductive lithology is the least possible explanation for the resistivity datasets. There are no known ultra-conductive ore deposits in the area, and no metallic deposits exist in the Nacimiento Fault which would cause convective signatures. Antithetical lithology on either side of a fault is highly unlikely. This explanation can also be discounted. Fluid-filled voids is the next possible explanation, though if this were the case at the site, the resistivity images would show highly resistive outlines filled with highly conductive inner spaces that are not seen in the data analysis.

The next explanation of the convective signatures is fluid upwelling of two fluids with an electrically conductive gradient. Upwelling from depth is not a plausible cause for the convective signals that exist at the field site. ERI and fluid chemistry data indicates that upwelling of relatively fresh water along the fault is occurring, though it cannot account for the conductive features obtained from the processed data. As the upwelling reaches the surface, it should become more dilute and the abnormally conductive areas should exist at the bottom of the ERI image and not in the mid-section. ERI line EWN100 does support the theory for upwelling. The only remaining explanation of the data gathered at the site involves haline free convection underneath the active mound spring Twin Mound East in the Nacimiento Fault Zone. The free convection explanation appears to fit the complete dataset.

Implications of Research

Future implications concerning this research include a further understanding of groundwater convective theory as well as a further understanding of water supply quality and ore body deposition in faulted hydrothermal ore deposits. Density-driven free convection affects landfill plumes, radioactive waste sites and deep faulted aquifers. Quantifying these processes will allow for a better ability to predict contaminant transport and related impacts on water quality and supply.

In order to further study the Tierra Amarilla mound springs site, transient imaging should be conducted at a timescale of hours instead of days in order to capture the rotation of Mode 2A and Mode 2B convective cells. In order to further study the Mode 1convection occurring at the site, a timescale of 4-8 weeks may be necessary to capture the convective rotation and further quantify the interfracture convective cells.

CHAPTER VII

CONCLUSIONS

A field study was conducted in north-central New Mexico, USA, to evaluate the potential for free convective groundwater flow in the Nacimiento Fault Zone. The study evaluated theoretical values for Rayleigh numbers to evaluate if the flow was unstable. Then fluid and electrical resistivity data were collected to evaluate if field evidence existed for free convection.

The results show circular conductive features which change over time as well as EC oscillations in transducer data. The data are supportive of the presence of Mode 1 and Mode 2B convection cells located adjacent to and inside the fault plane. The calculated Rayleigh number for Mode 1 free convection was 49.4, while the value for Mode 2 was 53.6; which is above the established theoretical values required for the onset of free convection. The Mode 1 convective cells have an average size of 195 meters and the Mode 2B convective cells have an average size of 128 meters. The Rose criteron was utilized to determine if a unique wavelength signal existed in the dataset. The method was supportive of the presence of convection cells. Free convection is assumed to exist at the site based upon the calculation of the Rayleigh number. Alternative hypotheses were not supported by the field data.

This study provides the first quantification of groundwater free convection cells in a fault, and the first evidence of antithetical Mode 1 cells in a hydraulically active fault zone. As these cells were

forming in fractured shale, these results have significant implications for the study of fluid flow in shales.

REFERENCES

Advanced Geosciences, Inc., 2004. Instruction Manual for EarthImager 2D Version 1.7.4 Resistivity and IP Inversion Software. P.O. Box 201087, Austin, Texas 78720. Tel. (512) 335-3338, Fax (512) 258-9958, www.agiusa.com

Andrews, R., Barker, R., and Heng, L., 1995. The application of electrical tomography in the study of the unsaturated zone in chalk at three sites in Cambridgeshire, United Kingdom. Hydrogeology Journal, Vol. 3, pp. 17-31.

Angisara, D., and Scrinivasan, J., 1989. Natural convection flows due to the combined buoyancy of heat and mass diffusion in a thermally stratified medium. J. Heat Transfer, 111, pp. 657-663.

Bagtzoglou, A., Lane, J.W., Cornacchiulo, D., and Ergun, K. 2003. Improved reconstruction of two-dimensional resistivity field data using geostatics. Geophysical Research Abstracts, Vol. 5, 30-1-2003.

Barker, T.B., 1990. *Engineering Quality by Design*. Marcel Dekker, New York, pp. 21-35.

Bauer, P., Supper, R., Zimmerman, S., and Kinzelbach, W., 2006. Geoelectrical imaging of groundwater salinization in the Okavango Delta, Botswana. Jrnl. Applied Geophysics 60, pp. 126-141.

Bénard, H., 1900. Les tourbillons cellulaires dans une nappe liquid, Rev. Gén. Sci. pures et appl. 11 pp. 1261-1271 and 1309-1328.

Bjorlykke, K., Mo, A., and Palm, E. 1988. Modeling of thermal convection in sedimentary basins and its relevance to diagenetic reactions. Mar. Pet. Geol., 5, pp. 338-351.

Cron, B., 2011. Geochemical characteristics and microbial diversity of CO_2-rich mound springs of the Tierra Amarilla anticline, New Mexico, Master's Thesis, pp.4-5, 46, 68.

Crook, N., Binley, A., Knight, R., Robinson, D.A., Zernetske, J., and Haggerty, R., 2008. Electrical resistivity imaging of the architecture of substream sediments. Water Resour. Research, Vol. 44, W00D13.

Cross M. C., and Hohenberg, P.C., 1993. Pattern formation outside of equilibrium. Rev. Mod. Phys., Vol. 65, No. 3.

Daily, W., Ramirez, A., Binley, A., and LaBrecque, D., 2004a. Electrical resistance tomography. The Leading Edge, v. 23, pp. 438-442.

Deng, Q.H., Zhou, J., Mei, C., and Shen, Y.M., 2004. Fluid, heat and contaminant transport structures of laminar double-diffusive mixed convection in a two-dimensional ventilated enclosure. Intl. Jrnl. of Heat and Mass Transfer, v. 47, pp. 5257-5269.

Dhu, T., Heinson G.S., Greenhalgh, S., Halihan, T., and Simmons, C.T., 2003. Environmental monitoring using electrical resistance tomography (ERT). 16th ASEG International Conference and Exhibition, Adelaide, Austrailia.

Diersch, H.-J. G., and Kolditz, O., 1996. Coupled groundwater flow and transport: 2. Thermohaline and 3D convection systems. Adv. Water Resour.,21, pp. 401-425.

Diersch, H.-J. G. and Kolditz, O., 2002. Variable-density flow and transport in porous media: Approaches and challenges. Adv. Water Resour., 25, pp. 899-944.

Elder, J.W., 1967. Transient convection in a porous medium. J. Fluid Mech., 27, pp. 609-623.

Fenstemaker, T.R., Halihan, T., Sharp Jr., J.M., 2001. Using resistivity to detect movements of variable salinity fluids in the barrier island sediments of Padre Island, Texas. Geological Society of America Abstracts with Programs 33 (6), A-46.

Freeze, R.A., Cherry J.A., 1979. *Groundwater*. Prentice-Hall, Englewood Cliffs, NJ.

Frind, E.O., 1982a. Seawater intrusion in continuous coastal aquifer-aquitard systems. Adv. Water Resour. 5, pp. 89-97.

Frolkovic, P., and De Schepper, H., 2000. Numerical modeling of convection dominated transport coupled with density driven flow in porous media, Adv. Water Resour.,24, pp. 63-72.

Ghebart, B., Jaluria, Y., Mahajan, R.L., and Sammakia, B., 1988. Buoyancy-induced flows and transport, Hemisphere/Harper and Row, New York.

Goosse, H., and Fichefet, T., 2000. Open-ocean convection and polynya formation in a large-scale ice-ocean model, Tellus Series A Dynamic Meteorology and Oceanography, 53 (1), pp. 94-111.

Graf, T., and Therrien R., 2007. Variable-density groundwater flow and solute transport in irregular 2D fracture networks, Adv. Water Resour., 30, pp. 455-468.

Jiang, P., 2004. Experimental research on convection heat transfer in sintered porous plate channels. International Journal of Heat and Mass Transfer 47, pp. 2085-2096.

Halihan, T., Puckette, ,J., Sample, M., and Riley, M., 2009. Electrical resistivity imaging of the Arbuckle-Simpson aquifer. OWRB Final Report.

Halihan, T., Crossey, L., Karlstrom, K., and Cron, B., 2011. ERI investigation of fluid flow in the Nacimiento Fault, New Mexico, American Geophysical Union, San Francisco, CA.

Halihan, T., Albano, J., Comfort, S.D., and Zlotnik, V.A., 2012. Electrical Resistivity Imaging of a Permanganate Injection During In Situ Treatment of RDX-Contaminated Groundwater. Ground Water Monitoring & Remediation, 32: pp. 43–52.

Halihan, T., and Fenstemaker, T.R., 2004. Proprietary Electrical Imaging Method, 2nd ed. Stillwater, Oklahoma: Oklahoma State University Office of Intellectual Property.

Hanna, T.M., and Harmon, E.J., 1989. An overview of the historical, stratigraphic, and structural setting of the aquifer system of the San Luis Valley, Colorado. Colorado Ground Water Association Field Trip Guidebook, pp. 1-34.

Holzbecher, E.O., 1998. Modeling density-driven flow in porous media. Berlin: Springer.

Horton, C.W., and Rogers, F.T., 1945. Convection currents in a porous medium. J. Appl. Phys. 16, pp. 367-370.

Hsu H.-L., Yanites, B. J., Chen C.-C., and Chen, Y., 2010. Bedrock detection using 2D electrical resistivity imaging along the Peikang River, central Taiwan, Geomorphology, 114 (3), pp. 406-414.

Huyakorn, P.S., Andersen, P.F., Mercer, J.W., and White, H.O., 1987. Saltwater intrusion in aquifers: development and testing of a three-dimensional finite element model. Water Resour. Res. 23 (2), pp. 293-312.

Karlstrom K., and Crossey, L., 2011. Discussion with the authors.

Kassem, T., 2007. Numerical study of the natural convection process in the parabolic-cylindrical solar collector. Desalination 209, pp. 144-150.

Kolditz, O., Ratke, R., Diersch, H.-J.G., and Zielke, W., 1996. Coupled groundwater flow and transport: 1. Verification of variable density flow and transport models, Adv. Water Resour.,21, pp. 27-46.

Lapwood, E.R., 1948. Convection of a fluid in a porous medium. Proc. Camb. Philos. Soc. 44, pp. 508-521.

Lee, C.-H., Cheng, R.T.-S., 1974. On seawater encroachment in coastal aquifers. Water Resour. Res. 10 (5), pp. 1039-1043.

Liu, X., Fehn, U., and Teng, R.T.D., 1997. Oil formation and fluid convection in Railroad Valley, NV: a study using cosmogenic isotopes to determine the onset of hydrocarbon migration. Nuclear Instruments and Methods in Physics Research Section B: Beam Interactions with Materials and Atoms, v. 123, pp. 356-360.

Love, A.J., Simmons, C.T., and Nield, N.A., 2007. Double-diffusive convection in groundwater wells, Water Resour. Res., 43, W08428.

McKenna, T.E., and Sharp Jr, J.M., 1997. Subsurface temperatures, fluid pressures, and salinities in the Rio Grande Embayment, Gulf of Mexico Basin, USA, Proc. Intl. Geol. Congr., Vol. 8, pp. 263-274.

Marshall, J., and Schott, F., 1999. Open-ocean convection: Observations, theory, and models. Rew Geophys 37, pp. 1-64.

Morgan, P., Harder, V., Daggett, P.H., and Swanberg, C.A., 1981. A groundwater convection model for Rio Grande rift geothermal resources.

Morton, R.A., and Land, L.S., 1987. Regional variations in formation water chemistry, Frio Formation (Oligocene), Texas Gulf Coast, AAPG Bull., 71, pp. 191-206.

Narayan, K.A., and Armstrong, D., 1995. Simulation of groundwater interception at Lake Ranfurly, Victoria, incorporating variable density flow and solute transport. Journal of Hydrology 165, pp. 161-184.

Nield, D.A., 1968. Onset of thermohaline convection in a porous medium, Water Resour. Res., 4(3), pp. 553-560.

Nield, D.A., 1994. Estimation of an effective Rayleigh number for convection in a vertically inhomogenous porous medium or clear fluid. Intl. Journal of Heat and Fluid Flow, Vol. 15, Issue 4, pp. 337-340.

Nield, D.A., Simmons, C.T., Kuznetsov, A.V., and Ward, J.D., 2008. On the evolution of salt lakes: Episodic convection beneath an evaporating salt lake, Water Resour. Res., 44, W02439.

Nield, D.A., and Kuznetsov, A.V., 2006. The effects of combined horizontal and vertical heterogeneity on the onset of convection in a porous medium. Intl. Jrnl. of Heat and Mass Transfer Vol. 50, Issues 9-10, May 2007, Pages 1909-1915.

Nield, D.A., and Kuznetsov, A.V., 2011. The effects of combined horizontal and vertical heterogeneity on the onset of convection in a porous medium with horizontal throughflow, Intl. Jrnl. of Heat and Mass Transfer 54, pp. 5595-5601.

Nield, D.A., and Bejan, A., 2006. Convection in porous media, 3rd ed., Springer, New York.

Nijland, W., van der Meijde, M., Addink, E.A., and de Jong, S.M., 2010. Detection of soil moisture and vegetation water abstraction in a Mediterranean natural area using electrical resistivity tomography. CATENA, Vol. 81, Issue 3, pp. 209-216.

Oostrom, C.M., Dane, J.H., Guven, O., and Hayworth, J.S., 1992a. Experimental investigation of dense solute plumes in an unconfined aquifer model. Water Resour. Res. 28 (9), pp. 2315-2326.

Pazzaglia, F.J., and Kelley, S.A., 1998. Large-scale geomorphology and fission-track thermochronology in topographic and exhumation reconstructions of the southern Rocky Mountains, Rocky Mountain Geology, v. 33, n.2, pp. 229-257.

Peña A.A., and Miller, C.A., 2006. Solubilization rates of oils in surfactant solutions and their relationship to mass transport in emulsions. Adv. in Colloid and Interface Science pp. 123-126 and 241-257.

Pilon, L., Zhao, G., and Viskanta, R., 2002. Three-Dimensional Flow and Thermal Structure in Glass Melting Furnaces. Part II: Effect of Batch and Bubbles. Glass Science and Technology, Vol. 75, No.3, pp. 115-124.

Pinder, G.F., Cooper, H.H., 1970. A numerical technique for calculating the transient position of the saltwater front. Water Resour. Res. 6 (3), pp. 875-882.

Pollock, C.J., Stewart, K.G., Hibbard, J.P., Wallace, L., and Giral, R.A., 2004. Thrust wedge tectonics and strike-slip faulting in the Sierra Nacimiento, New Mexico. New Mexico Bureau of Geology and Mineral Resources, Bulletin 160, 2004.

Rabinowicz, M., Dandurand, J-L., Jakubowski, M., Schott, J., and Cassan J-P. 1985. Convection in a north sea oil reservoir: influences on diagenesis and hydrocarbon migration. Earth and Planetary Science Letters, v. 74, pp. 387-404.

Rayleigh L., 1916. On the convective currents in a horizontal layer of fluid when the higher temperature is on the under side, Phil. Mag. 32 pp. 529-546.

Reynolds, J.M., 1997. An introduction to applied and environmental geophysics: Toronto, John Wiley & Sons, pp. 417-490.

Ronen, D., Yechieli, Y., and Kribus, A., 1995. Buoyancy-induced flow of a tracer in vertical conduits, Water Resour. Res., 31(5), pp. 1167-1174.

Schincariol, R.A., Schwartz, F.W., 1990. An experimental investigation of variable density flow and mixing in homogeneous and heterogeneous media. Water Resour. Res. 26 (10), pp. 2317-2329.

Segol, G., Pinder, G.F., 1976. Transient simulation of saltwater intrusion in Southeastern Florida. Water Resour. Res. 12 (1), pp. 65-70.

Segol, G., Pinder, G.F., Gray, W.G., 1975. A Galerkin-finite element technique for calculating the transient position of the saltwater front. Water Resour. Res. 11 (2), pp. 343-347.

Sharp Jr., J.M., Fenstemaker, T.R., Simmons, C.T., McKenna, T.E., and Dickinson, J.K., 2001. Potential thermohaline convection in a shale-rich sedimentary basin: Example from the Gulf of Mexico Basin in south Texas, AAPG Bull., 85, pp. 2089-2110.

Shikaze, S.G., Sudicky, E.A., and Schwartz, F.W., 1998. Density-dependent solute transport in discretely-fractured geologic media: Is prediction possible? J. Contam. Hydrol., 34, pp. 273-291.

Simmons, C.T., 2005. Variable density groundwater flow: From current challenges to future possibilities, Hydrogeol. J., 13(1), pp. 116-119.

Simmons, C.T., 2008. Sabkha free convective stability criteria, wavelength and timescales: Preliminary assessment of free convection spatial and temporal scales and their possible influence on geophysical experimental design. Personal communication with the author.

Simmons, C.T., and Sharp Jr., J.M., 2000. On variable-density groundwater flow in heterogeneous porous media, In:Proceeding of the XXX LAH Congress on Groundwater: Past Achievements and Future Challenges:, Cape Town, South Africa, Nov 26-Dec 1, 2000, O. Sililo et al. (eds), A. A. Balkema, Rotterdam, pp. 425-430.

Simmons, C.T., Fenstemaker, T.R., and Sharp Jr., J.M., 2001. Variable-density groundwater flow and solute transport in heterogeneous porous media: approaches, resolutions and future challenges. J. Contam. Hydrol., 52, pp. 245-275.

Simmons, C.T., Narayan, K.A., and Wooding, R.A., 1999. On a test case for density-dependent groundwater flow and solute transport models: The salt lake problem, Water Resources Research, 35(12), pp. 3607-3620.

Simmons, C.T., Pierini, M.L., and Hutson, J.L., 2002. Laboratory investigation of variable-density flow and solute transport in unsaturated-saturated porous media, Transp. Porous Media, 47, pp. 215-244.

Simmons, C.T., Sharp Jr., J.M. and Nield, D.A., 2008. Modes of free convection in fractured low-permeability media. Water Resources Research 44, W03431.

Simms, M.A., and Garven, G., 2004. Thermal convection in faulted extensional sedimentary basins: theoretical results from finite-element modeling. Geofluids 4, pp. 109-130.

Smith, R.C., and Sjogren, D.B., 2006. An evaluation of electrical resistivity imaging (ERI) in Quarternary sediments, southern Alberta, Canada. Geosphere: 2, pp. 287-298.

Stevens, J.D., Sharp Jr., J.M., Simmons, C.T., and Fenstemaker, T.R., 2009. Evidence of free convection in groundwater: Field-based measurements beneath wind-tidal flats. J. Hydrol. 375, pp. 394-409.

The University of Texas Hydrogeology Fields Methods Class, 1997. A hydrogeologic investigation of a transect across North Padre Island, Padre Island National Seashore, Kleberg County, Texas: Report to Padre Island National Seashore, 18 p. + appendices.

The University of Texas Hydrogeology Fields Methods Class, 2001. Hydrogeologic characterization of Padre Island National Seashore 28 km south of Corpus Christi, Texas: Report to Padre Island National Seashore, 41 p. + appendices.

The University of Texas Hydrogeology Fields Methods Class, 2003. A Hydrogeologic transect of North Padre Island: Laguna Madre to the Gulf of Mexico along Old Bird Island Basin Road, Kleberg County, Texas, USA: Report to Padre Island National Seashore, 16 p. + appendices.

The University of Texas Hydrogeology Fields Methods Class, 2005. Hydrogeologic characterization of Padre Island National Seashore near Corpus Christi, Texas: Report to Padre Island National Seashore, 47 p. + appendices.

The University of Texas Hydrogeology Fields Methods Class, 2007. Hydrogeologic characterization of Padre Island National Seashore near Corpus Christi, Texas: Report to Padre Island National Seashore, 47 p. + appendices.

Trendell, A. M., Atchley, S.C., and Nordt, L.C., 2012. Depositional and diagenetic controls on reservoir attributes within a fluvial outcrop analog: Upper Triassic Sonsela member of the Chinle Formation, Petrified Forest National Park, Arizona; The American Association of Petroleum Geologists, 2012.

Van Dam, R.L., Simmons, C.T., Hyndman, D.W., and Wood, W.W., 2009. Natural free convection in porous media: First field documentation in groundwater. Geophysical Research Letters 36, 1-5.

Van Reeuwijk, M., Mathias, S., Simmons, C.T., and Ward, J., 2008. Improving the worthiness of the Elder problem as a benchmark for buoyancy driven convection models. Available from Nature Precedings, http://dx.doi.org/10.1038/npre.2008.2633.1

Voss, C.I., and Souza, W.R., 1987. Variable density flow and solute transport simulation of regional aquifers containing a narrow freshwater-saltwater transition zone. Water Resour. Res. 23 (10), pp. 1851-1866.

Voss, C.I., 1984. SUTRA: A finite-element simulation model for saturated-unsaturated fluid density-dependent groundwater flow with energy transport or chemically reactive single-species solute transport, US Geological Survey Water Resources Investigations, Report 84-4369, 409 p.

Weatherhill, D., Simmons, C.T., Voss, C.I., and Robinson, N.I., 2004. Testing density-dependent groundwater models: Two-dimensional steady state unstable convection in infinite, finite and inclined porous layers, Adv. Water Resour., 27, pp. 547-562.

Wightman, W.E., Jalinoss, F., Sirles, P., and Hanna, K., 2003. Application of geophysical methods to highway related problems. Federal Highway Administration, Central Federal Lands Highway Division, Lakewood, CO, Publication No. FHWA-IF-04-021, September 2003.

Wooding, R.A., Tyler, S.W., and White, I., 1997a. Convection in groundwater below an evaporating salt lake: 1. Onset of instability, Water Resour. Res., 33, pp. 1199-1217.

Wooding, R.A., Tyler, S.W., White, I., and Anderson, P.A., 1997b. Convection in groundwater below and evaporating salt lake: 2. Evolution of fingers or plumes, Water Resour. Res., 33, pp. 1219-1228.

Woodward, L.A., 1987. Geology and mineral resources of Sierra Nacimiento and vicinity, New Mexico: New Mexico Bureau of Mines and Mineral Resources, Memoir 42, 84 p.

Woodward, L.A., and Ruetschilling, R.L., 1976. Geology of the San Ysidro quadrangle, New Mexico: New Mexico Bureau of Mines and Mineral Resources, Geologic Map 37, scale 1:24,000.

Woodward, L.A., Kaufman, W.H., and Anderson, J.B., 1971. Nacimiento fault and related structures, northern New Mexico GSA Bulletin August 1972 v. 83 no. 8 p. 2383-2396.

Zhiqiang, Y., and Zhihao, Z., 1997. Basic flow pattern and its variation in different types of glass tank furnaces", *Glastechnische Berichte*, vol. 70, pp. 165-172.

APPPENDICES

APPENDIX A

Table A.1: Reference table for equations

Symbol	**Description**	**Units**
A	cross sectional area	meters^2
b	fracture aperture	meters
ΔC	change in concentration	dimensionless
D	solute diffusivity	meters^2/second
D_{av}	effective diffusion coefficient	meters^2/second
d	plate separation	meters
g	acceleration due to gravity	meters/second^2
H	layer thickness	meters
I	current	amps
K	hydraulic conductivity	meters/second
k	permeability	meters^2
k	thermal diffusivity	meters^2/second
L	length	meters
R	resistance	ohms
Ra	Rayleigh number	dimensionless
Ra_{cr}	Rayleigh number (critical onset)	meters
ΔT	change in temperature	degrees Celsius
U_c	convective speed	meters/second
V	potential difference	volts
V_o	kinematic viscosity of the fluid	meters^2/second
v	kinematic viscosity of the fluid	meters^2/second
θ	aquifer porosity	dimensionless
$\beta = \partial\rho/\partial C$	linear expansion coefficient of fluid density/changing fluid concentration	dimensionless
λ	fracture spacing	meters
ρ	resistivity	ohm-meters

ρ	density	kilograms/meter^3
α	thermal expansion coefficient	meters/degrees Celsius

APPENDIX B

Figures Processed ERI lines from June, 2012

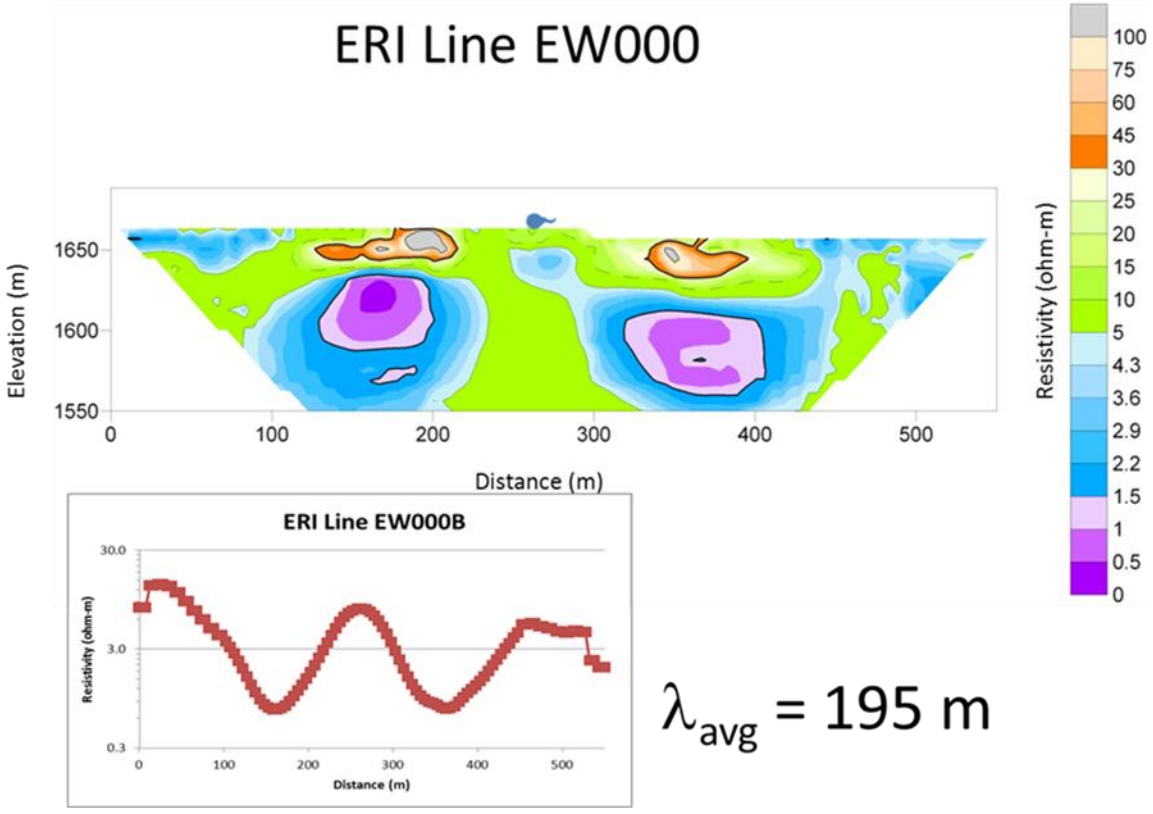

Figure B.1 ERI line EW000 showing highly conductive antithetical pinwheels on either side of the Nacimiento Fault with an average wavelength of 195 meters.

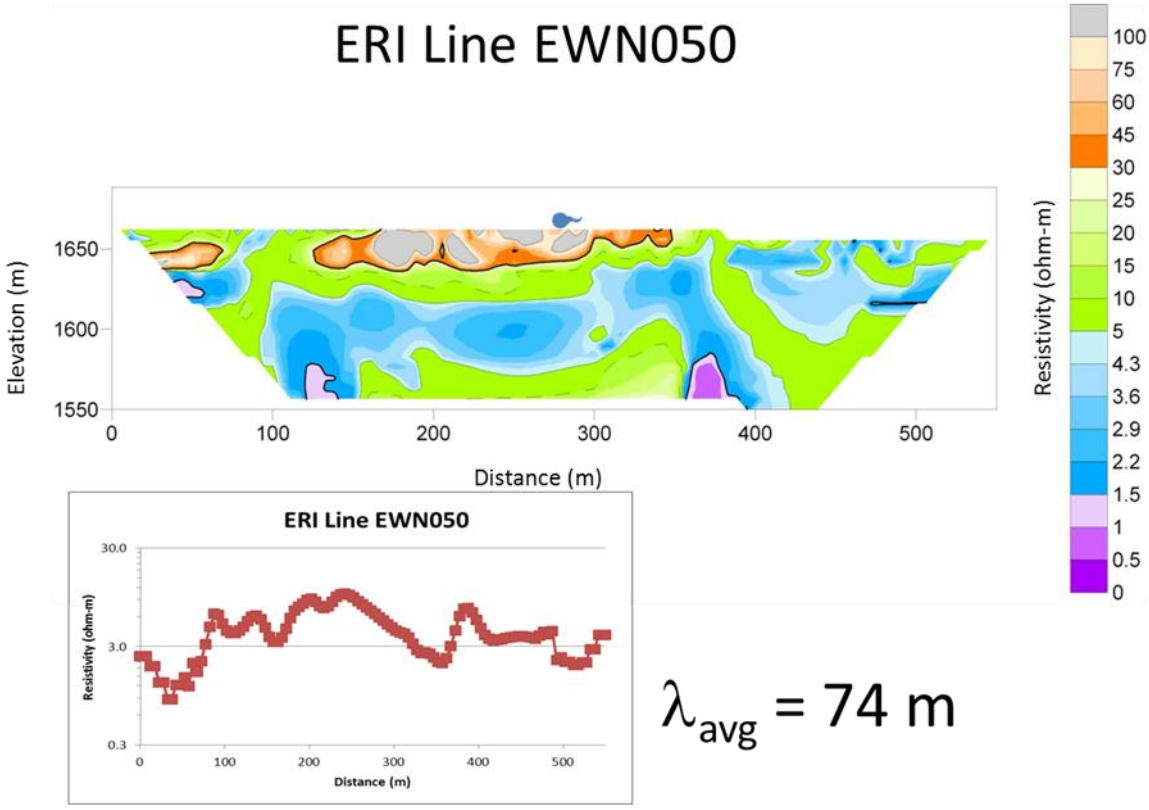

Figure B.2: ERI line EWN050 showing some convective cells with an average wavelength of 74 meters.

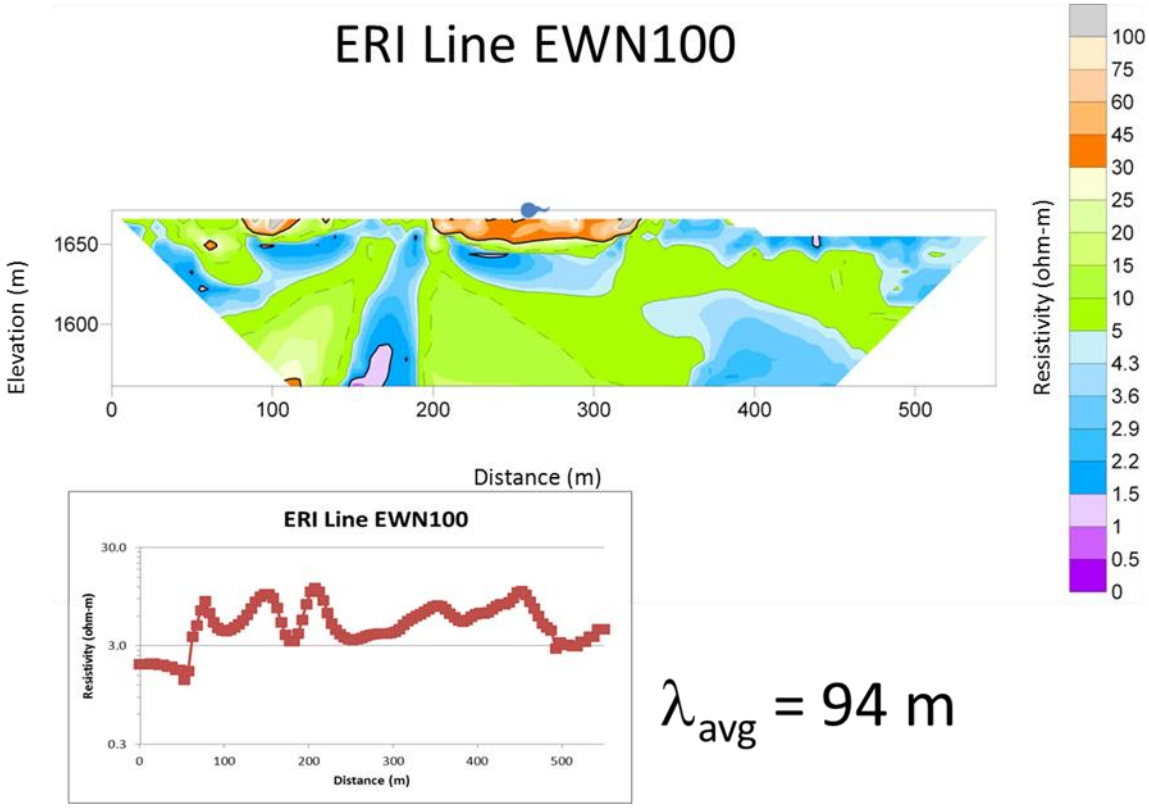

Figure B.3: ERI line EWN100 showing no convective cells with an average wavelength of 94 meters.

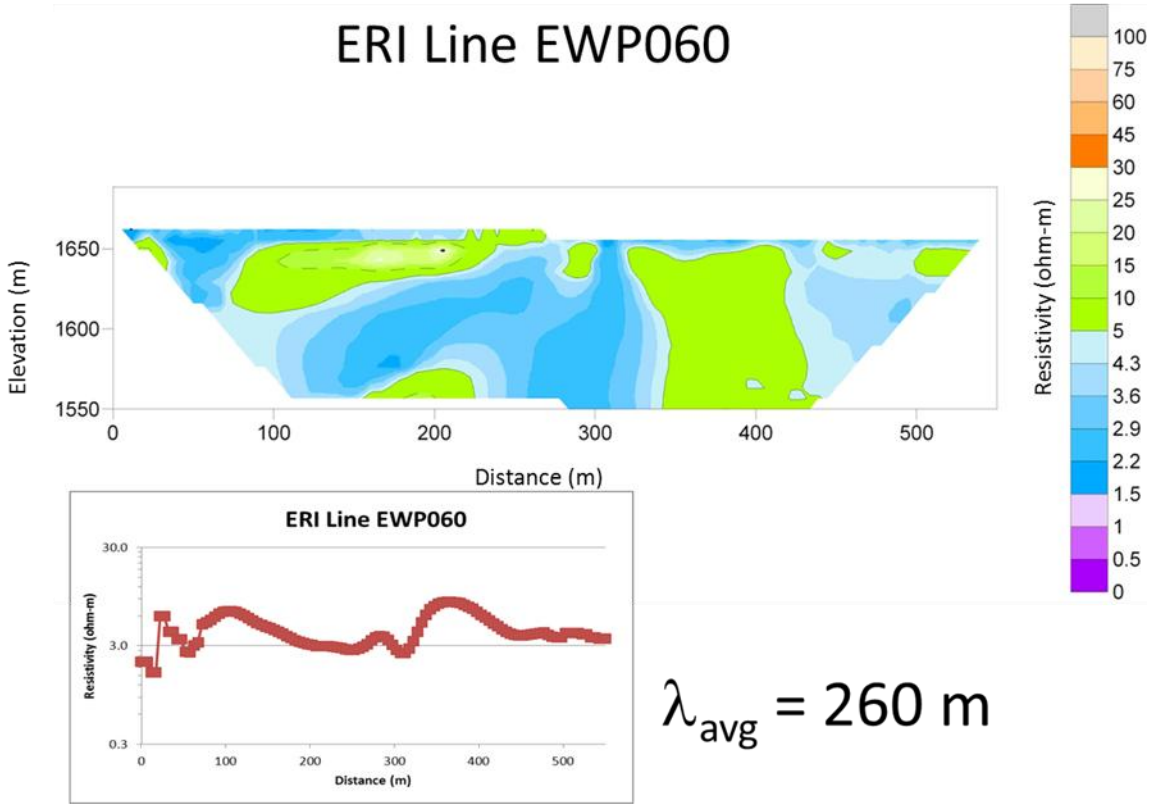

Figure B.4: ERI line EWP060 showing no convective cells with an average wavelength of 260 meters.

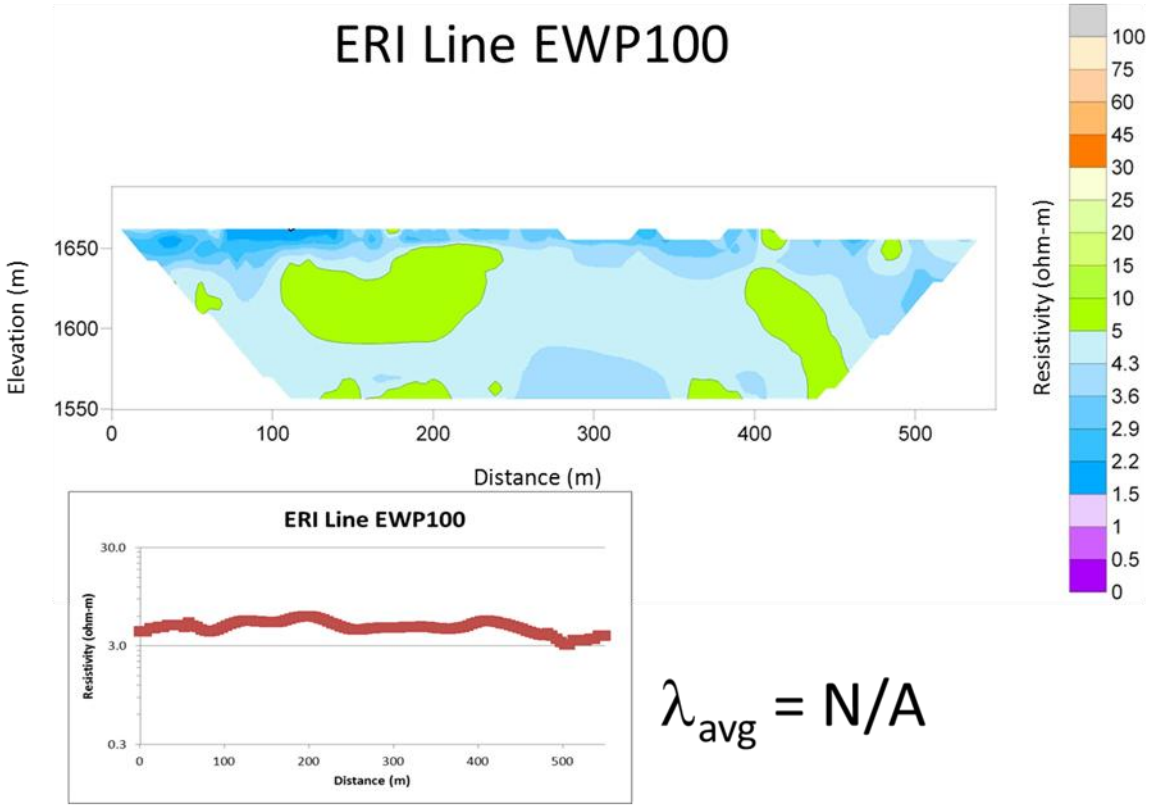

Figure B.5: ERI line EWP100 showing no convective cells. Utilizing the employed wavelength analysis and Rose criterion, no convective cells exist. The average wavelength is not applicable.

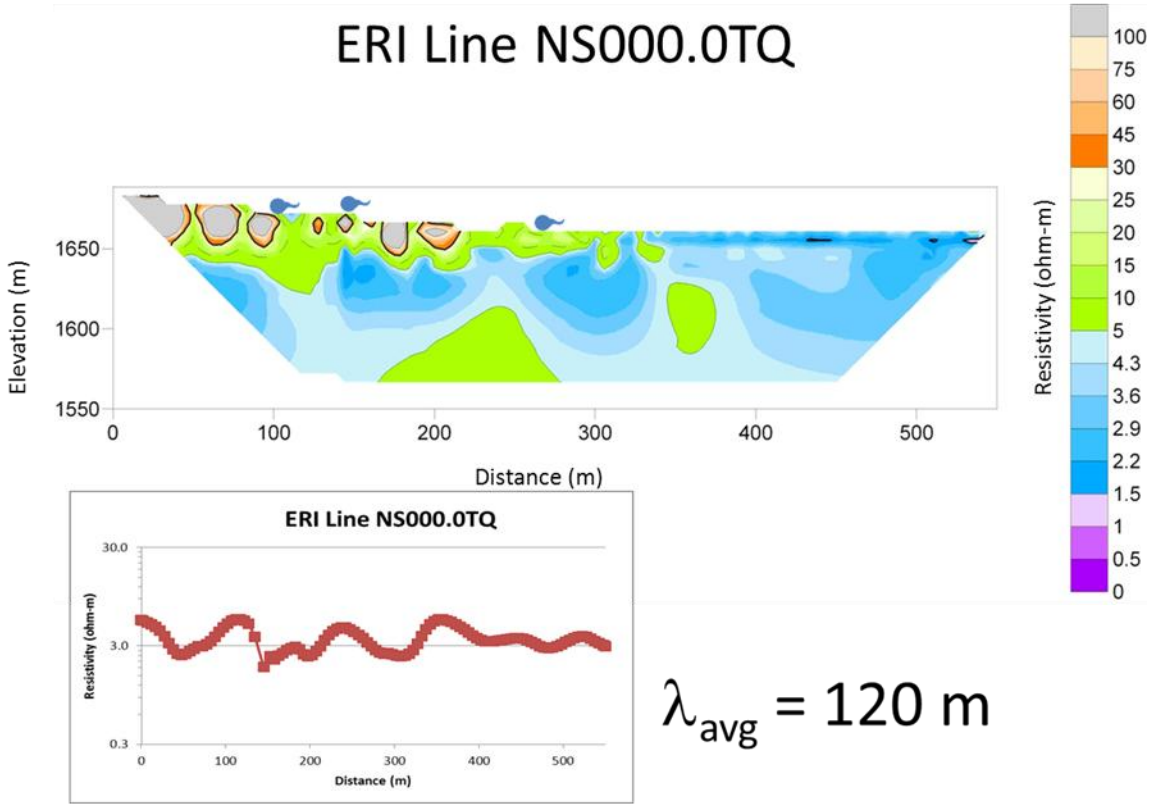

Figure B.6: ERI line NS000.0TQ showing expected convective cells with an average wavelength of 120 meters.

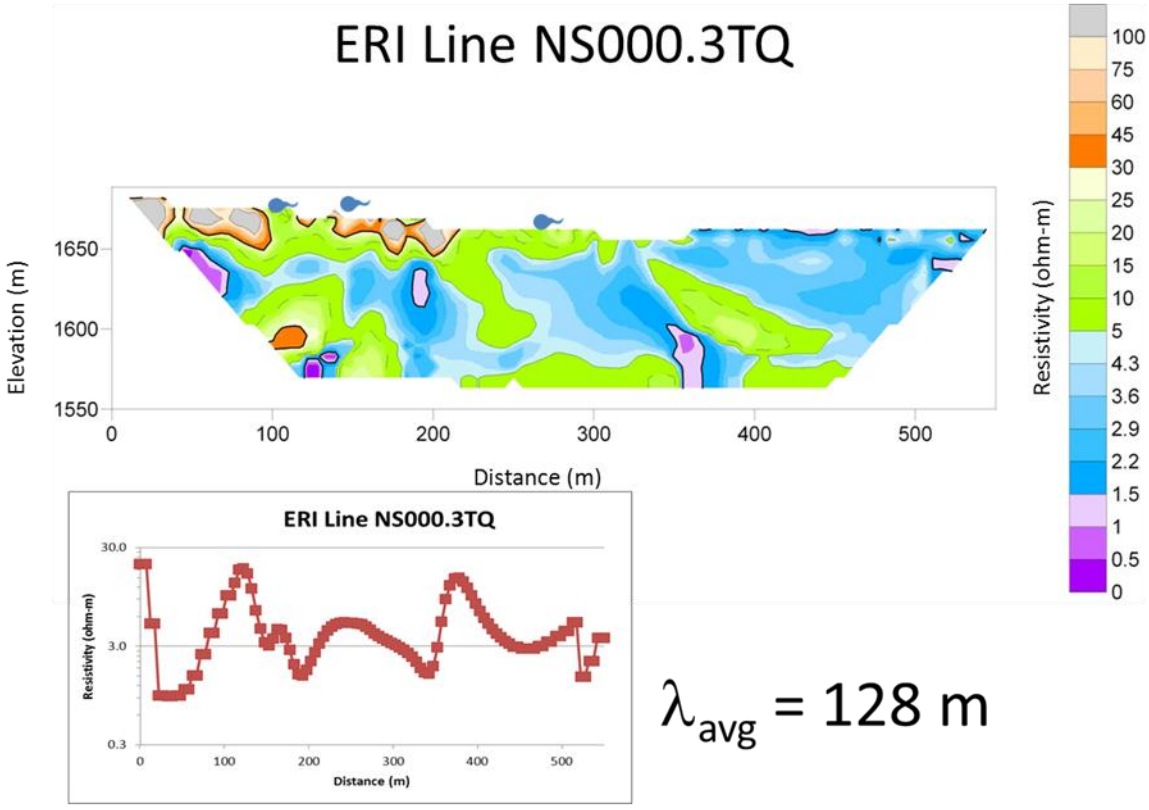

Figure B. 7: ERI line NS000.3TQ showing expected convective cells with an average wavelength of 128 meters.

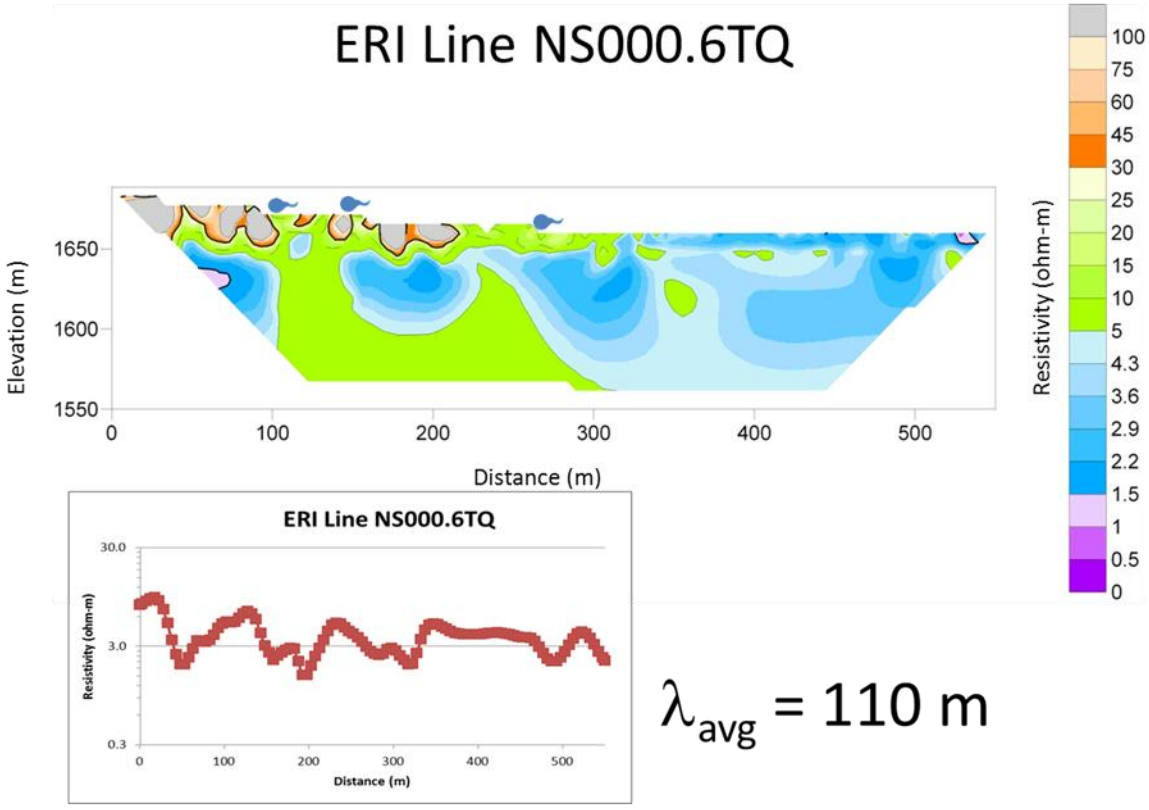

Figure B.8: ERI line NS000.6TQ showing expected convective cells with an average wavelength of 110 meters.

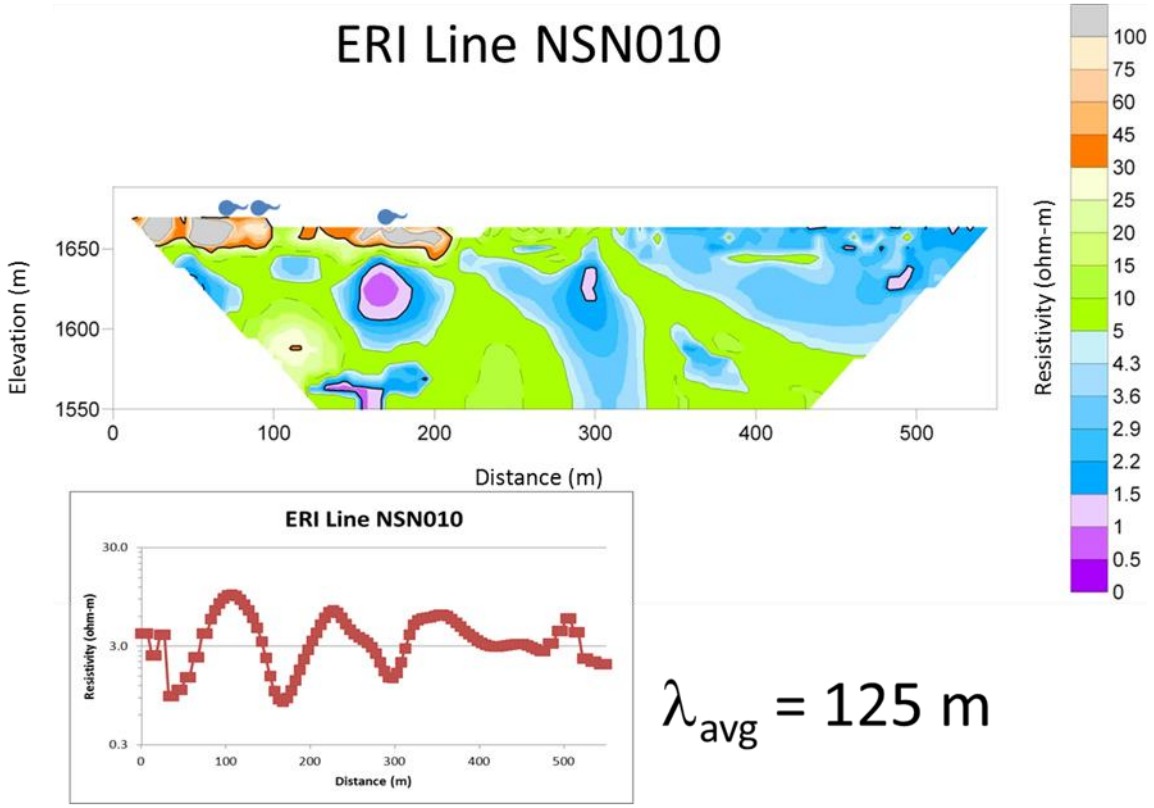

Figure B.9: ERI line NSN010 showing expected convective cells with an average wavelength of 125 meters.

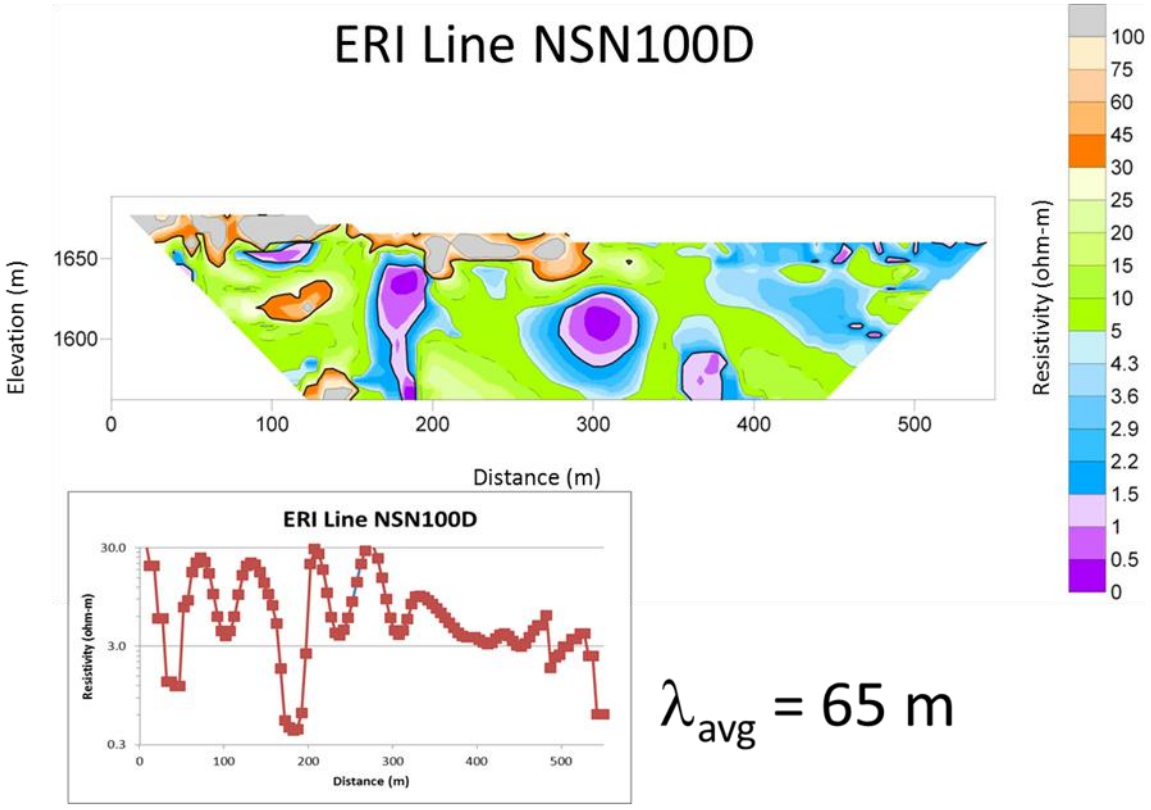

Figure B.10: ERI line NSN100D showing some convective cells with an average wavelength of 65 meters.

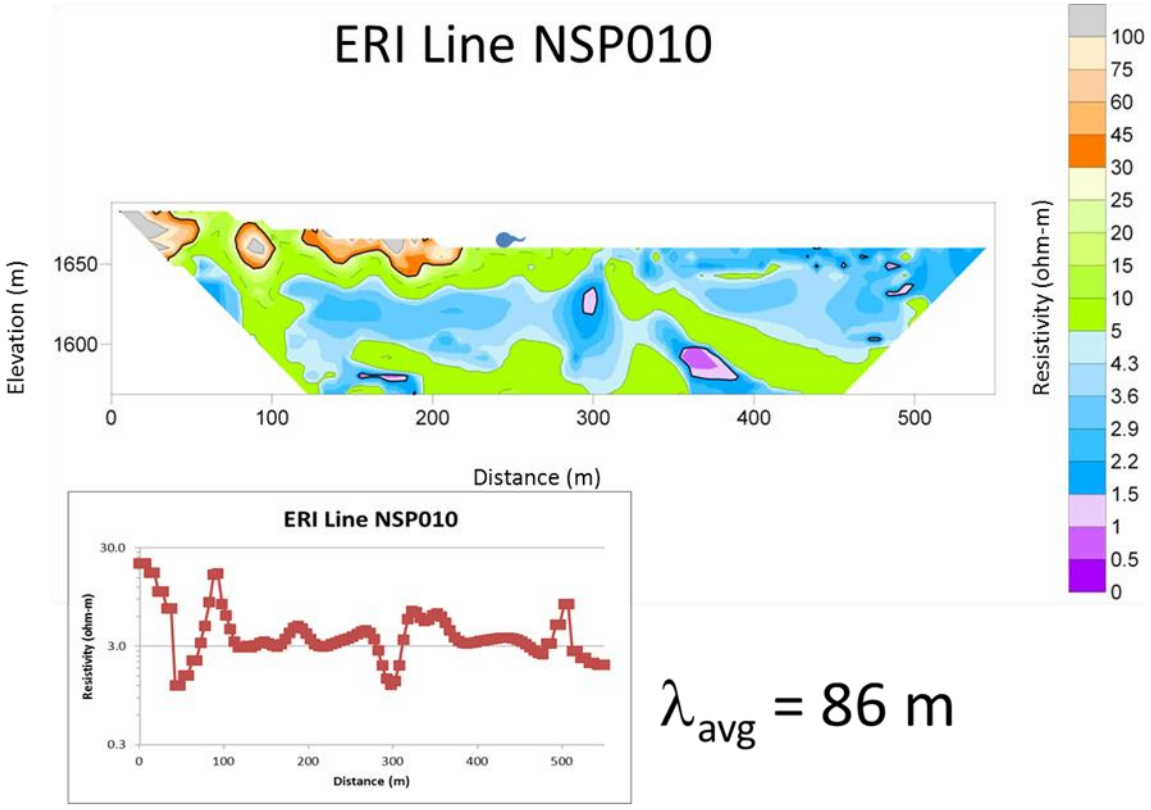

Figure B.11: ERI line NSP010 showing some convective cells with an average wavelength of 86 meters.

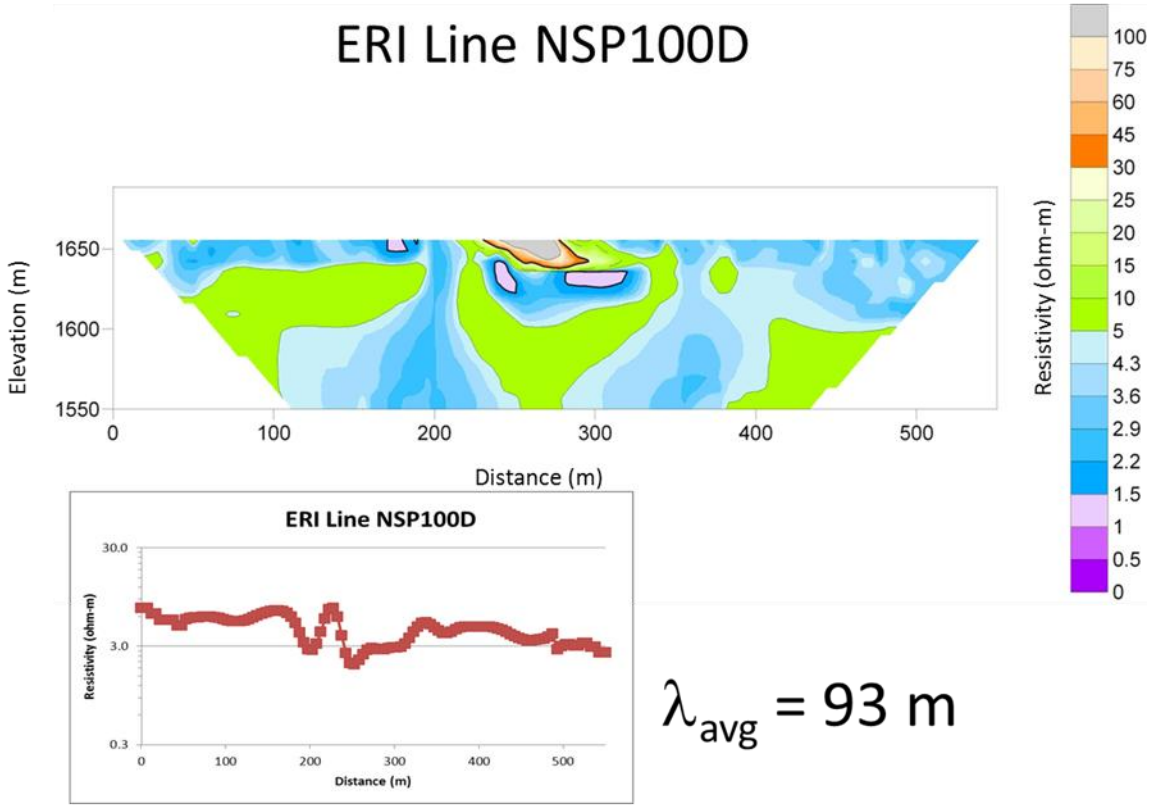

Figure B.12: ERI line NSP100D showing no convective cells expected with an average wavelength of 93 meters.

VITA

Robert Reynolds

304 N. Webster Ave. - Norman, Oklahoma, 73069 - (405)-924-4340
robert.reynolds@okstate.edu

Education

M.S., Environmental Science, Oklahoma State University – Stillwater, Oklahoma, Graduation: May 2013

Thesis: "Hydrogeological Evidence of Groundwater Convection in the Nacimiento Fault" – conducted hydrogeophysical evaluation of convection cells in a fault zone using resistivity and fluid data.

B.A., Psychology, B.A., Fine Arts Studio, University of Colorado – Colorado Springs, Colorado, December 2001

A.A., Environmental Science, Eastern Oklahoma State College – Wilburton, Oklahoma, May 1993

Experience

Research Assistant, Oklahoma State University, Geology Department

Stillwater, Oklahoma, June 2012 – July 2013

- Research Assistant with a team from Colorado State University and Oklahoma State University. "ERI Resistivity Survey on a Sand Tank LNAPL Experiment" funded by Chevron.

Groundwater Hydrologist, Thornhill Group Inc. Austin, Texas, May 2012

- Aquifer test using e-meters contracted through OG&E at the Lake Overholser Power Plant in Oklahoma City, Oklahoma

Grants And Publications

- GSA Research Grant for $1,300 received February 2012 for thesis field work
- PSO Environmental Science Graduate Program Research Assistantship for $1,000 received February 2012 to fund transportation for thesis work to be done in New Mexico
- Geological Society of America (GSA) Abstract: "Field Evaluation of Groundwater Convection in the Nacimiento Fault". Presented at the Austin, Texas regional conference April 2013
- Oklahoma Clean Lakes & Watersheds (OKCLW) Abstract: "Field Evaluation of Groundwater Convection in the Nacimiento Fault". Presented at Stillwater, Oklahoma conference April 2013

Name: Robert Reynolds Date of Degree: July 2013

Institution: Oklahoma State University Location: Stillwater, Oklahoma

Title of Study: "HYDROGEOPHYSICAL EVIDENCE OF GROUNDWATER CONVECTION IN THE NACIMIENTO FAULT"

Pages in Study: 93

Candidate for the Degree of Master of Science

Major Field: Environmental Science

Focus: Hydrogeology

Abstract:

Theory exists for unstable convective motion in porous and fractured media, and has been detected in the field as fluid fingers in porous media. Groundwater convective theory is limited though due to a lack of field evidence to understand and quantify the process of free convection in other settings such as faults. The Nacimiento Fault Zone in New Mexico was a suitable location for such a field study. This work provides quantification of haline convection in a hydraulically active fault zone. The hypothesis proposed that measured convective parameters of wavelength and timescales obtained from electrical resistivity and fluid data will correlate to convective groundwater theory in fault zones. Over a 2 year period (2011-2012), a total of 16 ERI lines provided two-dimensional and three-dimensional mapping of the convective fluid signatures in the Nacimiento Fault. Additionally, one line of transient data evaluated changes in the fault over a 6 day timescale. The results show circular conductive features which change over time as well as EC oscillations in transducer data.

ADVISER'S APPROVAL: Todd Halihan